JPRS L/8997

25 March 1980

USSR Report

ELECTRONICS AND ELECTRICAL ENGINEERING

(FOUO 5/80)

FBIS FOREIGN BROADCAST INFORMATION SERVICE

APPROVED FOR RELEASE: 2007/02/08: CIA-RDP82-00850R000200060038-2

NOTE

JPRS publications contain information primarily from foreign newspapers, periodicals and books, but also from news agency transmissions and broadcasts. Materials from foreign-language sources are translated; those from English-language sources are transcribed or reprinted, with the original phrasing and other characteristics retained.

Headlines, editorial reports, and material enclosed in brackets [] are supplied by JPRS. Processing indicators such as [Text] or [Excerpt] in the first line of each item, or following the last line of a brief, indicate how the original information was processed. Where no processing indicator is given, the information was summarized or extracted.

Unfamiliar names rendered phonetically or transliterated are enclosed in parentheses. Words or names preceded by a question mark and enclosed in parentheses were not clear in the original but have been supplied as appropriate in context. Other unattributed parenthetical notes within the body of an item originate with the source. Times within items are as given by source.

The contents of this publication in no way represent the policies, views or attitudes of the U.S. Government.

For further information on report content call (703) 351-2938 (economic); 3468 (political, sociological, military); 2726 (life sciences); 2725 (physical sciences).

APPROVED FOR RELEASE: 2007/02/08: CIA-RDP82-00850R000200060038-2

JPRS L/8997

25 March 1980

USSR REPORT

ELECTRONICS AND ELECTRICAL ENGINEERING

(FOUO 5/80)

This serial publication contains articles, abstracts of articles and news items from USSR scientific and technical journals on the specific subjects reflected in the table of contents.

Photoduplications of foreign-language sources may be obtained from the Photoduplication Service, Library of Congress, Washington, D. C. 20540. Requests should provide adequate identification both as to the source and the individual article(s) desired.

CONTENTS PAGE

Marine Radio Communications Ship Antennas
(OBZORNAYA INFORMATSIYA, SERIYA PROMYSLOVAYA RADIOELEKTRONNAYA APPARATURA I PODVODNAYA TEKHNIKA, SUDOVYYE ANTENNY MORSKOY RADIOSVYZAI, No 2, 1979)..... 1

Investigation of the Focusing Properties of Certain Second-Order Surfaces With the Incidence of a Plane Wave at an Angle to the Focal Axis
(M.G. Gorlov, L.B. Tartakovskiy; RADIOTEKHNIKA, No 10, 1979)... 3

Spectrum Analysis of Ultrashort Wave Signal Level in Long-Range Tropospheric Propagation Over an Ocean Route
(B.S. Rybakov; ELEKTROSVYAZ', No 10, 1979)..... 9

Depolarization of Radio Waves in Scattering on Vegetative Soil
(A.S. Skryabin; RADIOTEKHNIKA, No 10, 1979)..... 17

Approximate Determination of Statistical Distributions of Intensity of Rainfall
(Ye.A. Larin; ELEKTROSVYAZ', No 10, 1979)..... 29

Results of Tests of the 'Luch' Data Transmission Equipment on Vessels
(A.A. Borisovskiy; EKSPRESS-INFORMATSIYA, SERIYA PROMYSLOVAYA RADIOELEKTRONNAYA APPARATURA I PODVODNAYA TEKHNIKA, No 11, 1979) 36

CONTENTS (Continued) Page

Microwave Attenuation in a Line of Metal-Dielectric-Semiconductor-Metal Composition
(A.K. Balyko, A.S. Tager; RADIOTEKHNIKA I ELEKTRONIKA, No 8, 1979)..... 38

Consideration of Design and Technological Features in the Realization of an Electronically Tuned Matched Filter for the Selection of a Complex Signal
(N.I. Smirnov, Yu.A. Karavayev; IZVESTIYA VUZOV RADIOELEKTRONIKA, Vol 22 No 8, 1979)..... 45

Fifth International Symposium on Electromagnetic Compatibility Announced
(ELEKTROSVYAZ', No 10, 1979)..... 51

Discretely Controlled Ferromagnetic Elements for the Conversion of Electric Power Parameters
(DISKRETNO-UPRAVLYAYEMYYE FERROMAGNITNYYE ELEMENTY DLYA PREOBRAZOVANIYA PARAMETROV ELEKTROENERGII, 1979)..... 52

Oscillation Sources Based on Surface Acoustic Waves
(A.V. Ryzhkov; RADIOTEKHNIKA, No 10, 1979)..... 55

Some Aspects of the Design of Close-Range Noise Signal Radar Sets With Integrated Coverage
(V.V. Grigorin-Ryabov, et al; RADIOTEKHNIKA, No 10, 1979)..... 61

Some Features of the Depolarizing Properties of Radar Targets
(L.A. Zhivotovskiy; RADIOTEKHNIKA, No 10, 1979)..... 67

Doppler Filtration in HF Direction-Finding in Combination With a Method of Analytic Beam Separation
(Yu.M. Agafonnikov, et al; RADIOTEKHNIKA I ELEKTRONIKA, No 8, 1979)..... 72

Distortions of the Radar Characteristics of Complex Objects When Exposed to a Spherical Wave
(V.M. Shlyakhin; RADIOTEKHNIKA, No 10, 1979)..... 81

Synthesis of a Single-Pulse Discriminator for a Located Target
(N.Ya. Kuz'; RADIOTEKHNIKA I ELEKTRONIKA, Vol 24 No 4, 1979)... 86

UDC 621.396.676:629.783

MARINE RADIO COMMUNICATIONS SHIP ANTENNAS

Moscow OBZORNAYA INFORMATSIYA, SERIYA PROMYSLOVAYA RADIOELEKTRONNAYA APPARATURA I PODVODNAYA TEKHNIKA, SUDOVYYE ANTENNY MORSKOY RADIOSVYAZI in Russian No 2, 1979 signed to press 3 May 79 pp 1, 47

[Annotation and table of contents from book by S.F. Makarova TsNIITEIRKh [Central Scientific Research Institute of Information and Technical and Economic Research of the Fish Industry], 47 pages]

[Text] The principles of organization of marine radio communications, the requirements for equipment and the stipulations for its use have important distinctive features, as compared with radio communications over land. These features are caused primarily by the not too large dimensions of antennas, the limited possibilities for placing them on vessels, and the need for equipment to operate over a broad frequency range with a continuous change in the coordinates of one correspondent (in ship to shore communications) or both correspondents (in ship to ship communications). The structure and types of ship antennas depend on the goals confronting marine radio communications.

The International Radio Consultative Committee (MKKR) has assigned the following frequency bands for marine communications: MF--405 to 535 kHz; HF--1605 to 3800 kHz and 4.063 to 25.600 MHz; and VHF--156 to 174 MHz. The 1605 to 3800 kHz frequency band is customarily called the "intermediate wave" (PV) band.

CONTENTS Page

MF-Band Antennas	1
HF Antennas	8
Some Methods of Improving the Efficiency of Ship MF and HF Antennas	17
VHF Antennas	23
Driven Antennas	28
Ship Antennas for Communications via Satellite	31
Problems of installing satellite communications antennas on fishing vessels	32
Types of supports for antennas	35

Methods of regulating the position of an antenna 37
Parameters of ship antennas 38
Experimental models of ship satellite communications antennas 40
Conclusions 43
Bibliography 44

CSO: 1860
8831

UDC 621.396.677.83

INVESTIGATION OF THE FOCUSING PROPERTIES OF CERTAIN SECOND-ORDER SURFACES WITH THE INCIDENCE OF A PLANE WAVE AT AN ANGLE TO THE FOCAL AXIS

Moscow RADIOTEKHNIKA in Russian No 10, 1979 pp 65-67 manuscript received after completion, 4 Sep 78

[Article by M.G. Gorlov and L.B. Tartakovskiy]

[Text] In selecting the optimal focusing surface for scanning reflector antennas it is necessary to know the dependence of the field strength at the focusing point and of the amplitude-phase distribution of the field in a focused spot near different surfaces on the geometry of the reflector and on the angle of incidence of a plane wave onto it. For the purpose of determining the characteristics of the focusing spot, let us consider the work of the reflecting surface in the reception mode [1]. Diffraction corrections for the close-range zone are not taken into account. Concretely, the problem is formulated in the following manner. Given are a symmetric focusing surface with a square aperture, L X L (fig 1), its orientation in space, and the direction of arrival of the plane wave. The focused field of the antenna is calculated from points determined in the approximation $2[\bar{n}, \bar{H}_{\text{pad [incidence]}}]$.

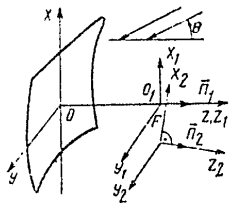

Figure 1.

Results of Calculation

Numerical calculations were made for symmetric focusing surfaces in the form of a paraboloid of revolution, a sphere and a parabolic torus, whose aperture equals 50λ X 50λ.

In cross section through plane xoz (fig 1) the parabolic torus represents part of a circle, and in the cross section through plane yoz , a parabola. Polarization is linear and vector E is placed in plane xoz .

In fig 2 are given calculated curves characterizing the shift in the focusing point in relation to the geometrical focus in a parabolic reflector when a plane wave strikes the reflector along the focal axis, as a function of F/L for different L/λ , where L is the linear dimension of the reflector's aperture. This shift is explained by the fact that when the observation point departs from the geometrical focus in the direction of the focusing surface, the amplitude of the field reflected from the reflector increases, but then a phase error is evidenced. For long-focus reflectors with a low ratio of L/λ the influence of the phase shift is slighter; therefore the maximum field concentration is produced at a point shifted toward the reflector; this shift increases with an increase in F/L and a reduction in L/λ .

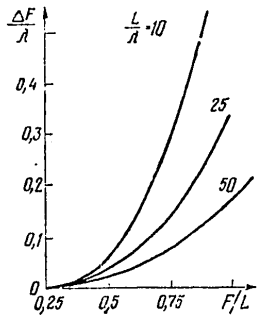

Figure 2.

In fig 3 is given the relative variation in the field at the focusing point at different surfaces as a function of F/L with θ = 0 (F is the distance from the focusing point to the vertex of the reflecting surface and θ is the angle of incidence of the plane wave onto the reflector). A parabolic reflector with F/L ≥ 1 (curve 1) can be replaced by a sphere (curve 2) or a parabolic torus (curve 3), and the energy at the focusing point drops by a total of about 0.4 dB. In order to maintain the same ratio of F/L (i.e., for focusing to occur at the same distance from the

vertex of the surface) for the focusing surfaces considered, it is necessary to select for each value of F/L its own radius for the sphere and radius for the circle of the parabolic torus. Here we will assume that $F_{\text{par. tora [parabolic torus]}} = F_{\text{paraboloida [paraboloid]}}$. Curves 4 and 5 characterize the dependence of R_{sf}/F and $R_{p.t}/F$ on F/L for a sphere and parabolic torus, respectively. In terms of its focusing properties the parabolic torus is inferior to the sphere. This can be explained by the fact that the radius of the sphere is always smaller than the radius of the parabolic torus's circle upon condition that the distance from the focusing point to the vertex is the same.

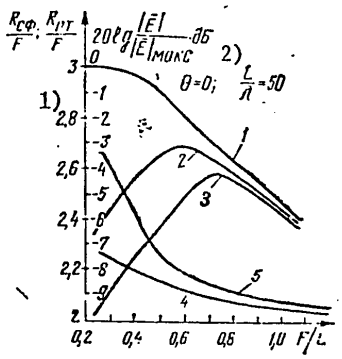

Figure 3.

Key:

1. $R_{sf\ [\text{sphere}]}/F$; $R_{p.t\ [\text{parabolic torus}]}/F$
2. $20 \log (|\bar{E}|/|\bar{E}|_{max})$, dB

It should be mentioned that by varying $F_{\text{par. tora}}$ ($F_{\text{par. tora}} \neq F_{\text{par}}$) and $R_{\text{par. tora}}$ it is possible to select a parabolic torus with the same ratio of F/L which will focus better than a sphere.

In fig 4 are given the trajectories of movement of the exciter, on which are plotted values of parameter θ for different focusing surfaces. The designations on curves 1, 2 and 3 are similar to the designations in figs 3-6. With an angle θ of from 0 to 8° the trajectories are close to one another and pass almost perpendicularly to the focal axis.

The curves in fig 5 characterize the dependence of the dimensions of the focusing spot on angle θ for the -3 dB level (curves 1, 2 and 3) and the -10 dB level (curves 4, 5 and 6) in the scanning plane. The dimensions of the focused spot vary chiefly in the scanning plane, and for a

parabolic torus its dimensions in the $\pm$ 14° scanning sector remain practically unchanged.

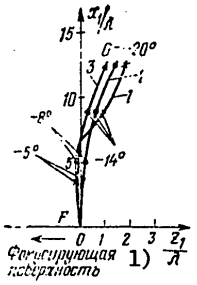

Figure 4.

Key:
1. Focusing surface

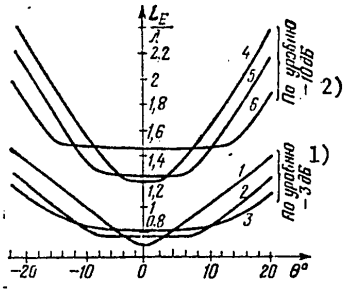

Figure 5.

Key:
1. For -3 dB level
2. For -10 dB level

In fig 6 is given the relative distribution of the flux of Poynting's vector (curves 1 to 3) and of the phase in the focused spot (curve 4 for a paraboloid, 5 for a sphere and 6 for a parabolic torus) in the scanning plane for $\theta = -20°$. The focused spot with a change in angle θ in the scanning plane becomes asymmetric both in terms of the level of side lobes and of the distribution of the phase.

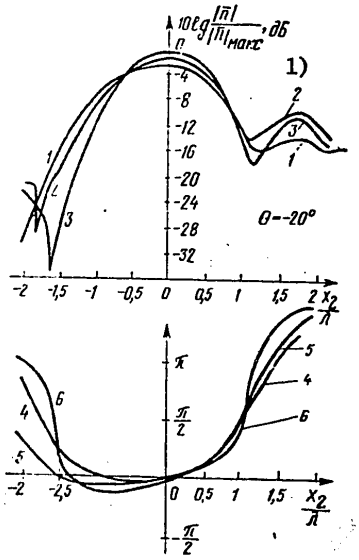

Figure 6.

Key:

1. 10 log $(|\bar{n}|/|\bar{n}|_{max})$, dB

Conclusions

1. With the normal incidence of a plane wave onto a paraboloid of revolution, the point with the maximum concentration of focused energy shifts from the geometrical focus in the direction of the reflector, and the more long-focus the system is and the smaller the ratio of L/λ , the greater this shift.

2. With the normal incidence of a plane wave onto a paraboloid of revolution, a sphere and a parabolic torus, with F/L from 0.25 to 1.1, with $F/L = 0.25$ a paraboloid has the greatest focusing properties. With $F/L \geq 1$, the focusing properties of the surfaces discussed are approximately identical.

Bibliography

1. Rusch, W.V.T. and Ludwig, A.C. TRANS. IEEE, Vol AP-21, No 2, 1973.

[59-8831]

CSO: 1860
8831

UDC 621.317.757

SPECTRUM ANALYSIS OF ULTRASHORT WAVE SIGNAL LEVEL IN LONG-RANGE TROPOSPHERIC PROPAGATION OVER AN OCEAN ROUTE

Moscow ELEKTROSVYAZ' in Russian No 10, 1979 pp 45-48 manuscript received 6 Mar 79

[Article by B.S. Rybakov]

[Text] Introduction

Intermittent fluctuations in the signal level in the long-range tropospheric propagation (DTR) of ultrashort waves (UKV's) are customarily divided into rapid and slow, distinguishing between 24-hour and seasonal variations [1]. Such a distinction is, firstly, arbitrary, and, secondly, some of the characteristics, as 24-hour and seasonal variations, for example, only qualitatively characterize the spectral structure of fluctuations in signal level. It would be interesting to investigate the spectrum of microwave signal fluctuations in DTR in terms of a long-duration realization (a few years) from the viewpoint of an analysis of non-steady-state random processes (NSP's) [2,7]. Unfortunately, the spectrum analysis of NSP's is a difficult problem which to a great extent has not been solved either theoretically or from the equipment viewpoint [2,4,7]. The concept of the energy spectrum of NSP's is defined variously [7,8].

In this paper, within the framework of the correlation theory, an attempt is made to estimate the spectrum properties of the level of a microwave DTR signal over an ocean route 225 km long, in terms of its annual realization, based on the property of "local stationarity" of the process [2].

Method of Calculating Spectrum

Realization of the process can be characterized by a set of local probability characteristics [2]:

$$\theta_j^* = \frac{1}{T_\theta} \int_{t_j}^{t_{j+1}} g\,[x(t')\,dt',\ t_j = jT_\theta\ ,\ j = 0,1,2,\ldots,N, \tag{1}$$

where $g[x(t)]$ is the estimate's operator; N is the whole part of the ratio T/T_θ ; T is the length of the realization, $x(t)$; and T_θ is the segment of time in which an estimate is made of $\theta^*(T_\theta)$, which does not exceed the interval of local stationarity of the process.

The application of algorithm (1) for the purpose of calculating the probability characteristics of rapid fluctuations is familiar [1]. The results of estimates in each segment (T_θ = 1 to 3 min) have furthermore been systematized in terms of some feature relative to the length of the realization.

In analyzing slow fluctuations, to initial process $x(t)$ can be applied a smoothing operator [2]:

$$C_{T_н}[x(t)] = \frac{1}{T_н}\int_{t-T_н}^{t} x(t')\,dt',\ T_н < t' < T \tag{2}$$

with the subsequent employment of algorithm (1).

The algorithm for estimating the spectrum of fluctuations of a non-steady-state process employed below is based on the successive multiple application of (1) and (2) to the measured realization of $x(t)$. As functional operator $g[x(t)]$ for the purpose of estimating the spectral power density, $\hat{G}(f)$, was selected the method in [3], based on an estimate of the correlation function with the subsequent employment of a Fourier transform. The selection of this method was due to the fact that it provides an asymptotically unbiased estimate of spectral density [3], and the intermediate results of calculation of correlation function $\hat{K}(t)$ are of independent interest.

The procedure for spectrum analysis thus reduces to the following. After the j-th cycle for applying operator (2), the realization of "smoothed" process $x_j(t)$, $0 \leq t \leq T$, is divided into N_j sections of length $T_{\theta j}$, in each of which is made a calculation of $\hat{K}_{ji}(t)$ and $\hat{G}_{ji}(f)$. Here $i = 1,2,3,\ldots,$ and N_j designates the number of the realization segment being processed. The variance in the curves for correlation functions $\hat{K}_{ji}(\tau)$, of course, causes considerable instability over time in local ("instantaneous") spectra of fluctuations, $\hat{G}_{ji}(f)$. In this connection, it has been considered [1,5] that it is advisable for the purpose of practice to consider averaged (in terms of the realization length) characteristics of the signal and, consequently,

$$\hat{\bar{K}}_j(\tau) = \sum_{i=1}^{N_j} \hat{K}_{ji}(\tau);\ \hat{\bar{G}}_j(f) = \sum_{i=1}^{N_j} \hat{G}_{ji}(f). \tag{3}$$

Then, to realization $x_j(t)$ is again applied operator (2) and process $x_{j+1}(t)$ with $0 \leq t \leq T$ is processed similarly. Algorithms (1) and (2) can be implemented either with a computer in processing data, or by the instrument method [7].

Estimates (3) characterize the averaged correlation and spectral properties of the process in a definite frequency band, $[f_{vj}, f_{nj}]$. By the selection of parameters T_{0j} and T_{ij} it is possible to ensure that estimates of $\hat{G}_j(f)$ for adjacent cycles of j and $j+1$ have regions which overlap with regard to frequency, $f_{v(j+1)} > f_{nj}$. Then set $\overset{M}{G}_j(f)$, $j = 1,2,3, \ldots,k$ in the sense defined above will characterize the spectrum of fluctuations of the measured process.

Calculation Results

Calculations were made according to the measurement data in [10], processed and systematized with the traditional approach (24-hour and seasonal variations, etc.). The conditions for conducting the experiment, as well as the characteristics of the measuring complex are described in the study indicated. Of importance here is the routine for recording the results of measurements, which were made in two-month cycles: February-March, May-June, August-September and November-December 1973. Within a cycle the signal level was measured daily in the morning (0800 to 1200), daytime (1400 to 1800), evening (2000 to 2400) and nighttime (0200 to 0600) hours.

The results of measurements for sessions lasting 1.5 to 3 h were recorded on an NO-36 tape recorder (sessions of type I) and on an automatic recording instrument (type II) with an upper frequency limit of 30 and 5 Hz, respectively. The data of sessions of type I were entered into the computer after digitizing the process in terms of time with an interval of $\Delta t = \tau_0/(5$ to $10)$ and in terms of level for 128 gradations of its dynamic range, and for sessions of type II, after the formation of mean-minute sampling values (τ_0 is the process's time correlation interval).

The processing of sampled values in both cases was carried out in keeping with the procedure described above, but in order to reveal, in particular, the correlation and spectral properties of the signal level at intervals frequently cited in the published data [1,5]. The parameters of some averaging and processing cycles are illustrated in the table. The 0.5 to 3 min section corresponds to the interval for the stationarity of rapid fluctuations [1], the 1.5 to 3 h segment was selected as the stationarity interval (prior to the appearance of a 24-h variation) for mean-minute values, and the 5 to 7 24-h-period segments, for mean hourly values, is contained within the limits of the synoptic period [6]. T_{0j} was selected within the limits indicated in the table for a specific realization segment, in keeping with the stationarity test in [4].

The results of calculation of the averaged spectra, $\overset{M}{G}_{j(f)}$, for different time intervals are given in fig 1, where the designations of the curves

correspond to the number of the subscript, j , of the averaging cycle. The spectral power density, $\overset{M}{G}_6(f)$, is a Fourier transform of the correlation function (fig 2d) computed for a yearly realization of 83 sampled values, averaged for three 24-h periods, of the signal level. Curve $\overset{M}{G}_5(f)$ is the averaged spectrum of fluctuations of mean 24-h values of the signal level in two-month measuring cycles: February-March, May-June, August-September and November-December.

Table

Length of segment, $T_{\theta j}$	Digitization interval, Δt_j	Sampled values, $x_j(k\Delta t_j)$	Sampled values, $x_{j-1} \rightarrow \rightarrow (k\Delta t_{j-1})$	Number of averaging segments, N_j
0.5 to 3 min	0.05 to 0.5 s	Measured (type I)	-	2000
1.5 to 3 h	1 min	Mean-minute	Measured (type II)	195
5 to 7 24-h periods	1 h	Mean hourly	Mean minute	22
1 year	3 24-h periods	Average for 3 24-h periods	Mean hourly	1

The correlation functions for each cycle are given in fig 2a by curves 1, 2, 3 and 4, respectively, and the correlation function averaged for them, $\overset{M}{K}(\tau)$, is given in fig 2b. The correlation function for mean hourly values of the signal level in 5 to 7 24-h intervals, averaged for 22 segments of the yearly realization, is given in fig 2c, and the corresponding spectral density is illustrated in fig 1 by curve 4.

The illustrations in fig 3 represent the results of calculating averaged correlation functions in terms of mean-minute sampled values in 1.5- to 3-h intervals for different months. The number of averaging segments equals 26 in May, 19 in August, 29 in September, 68 in November and 53 in December with a total number of sampled values greater than 20,000. The averaged spectral density corresponding to them is given in fig 1 by curve 3. The spectral densities, $\overset{M}{G}_2(f)$ and $\overset{M}{G}_1(f)$, of rapid fluctuations in the signal level in minute time intervals obtained by averaging for 2000 segments are illustrated by curves 2 and 1, respectively.

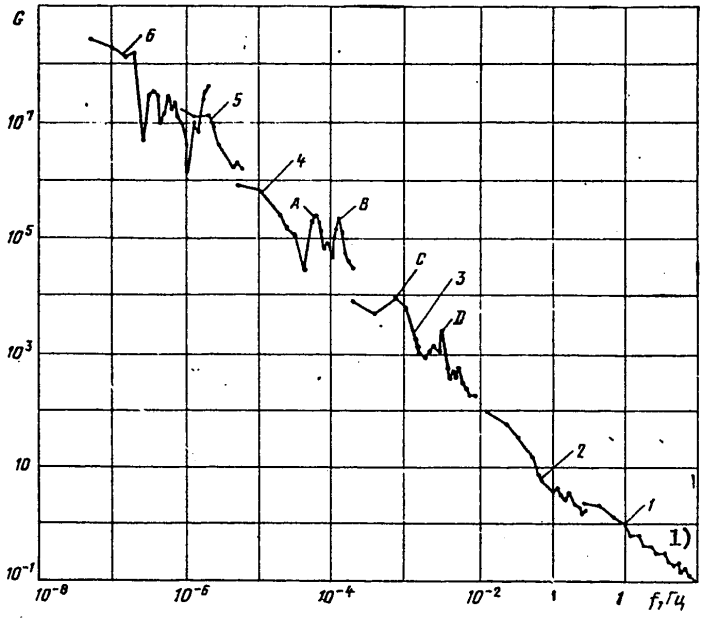

Figure 1.

Key:
1. f , Hz

The lack of agreement of curves $G_j^M(f)$ and $G_{j+1}^M(f)$ at the "boundary" is explained firstly by the different amount of averaging for the set of segments and consequently by the non-identical degree of reliability of the estimates obtained and, secondly, by the fact that the resolution of a spectrum analysis for different $G_j^M(f)$ is non-identical (by virtue of the method chosen for calculating the spectrum, and with a growth in j equals, respectively, $2.5 \cdot 10^{-1}$, $5 \cdot 10^{-2}$, $2.08 \cdot 10^{-4}$, $6.33 \cdot 10^{-6}$, $4.83 \cdot 10^{-7}$ and $1.93 \cdot 10^{-8}$ Hz. As is obvious, at the "boundaries" the frequency resolution changes by approximately an order of magnitude, and consequently estimates of spectral density relating to a single frequency but belonging to different curves have not been computed under equivalent conditions. This fact is important for the purpose of isolating peaks of the spectral power density reflecting "periodic" changes in the signal level.

The distinctly pronounced spectral density peak with tip A (fig 1) corresponds to a 24-h variation, and the peak with tip D, to its second harmonic. The sharp-point nature of both spectral density peaks, of approximately

identical shape, characterizes the "regularity" of the 24-h variation over the course of a year. Spectral density peaks with tips C and D, respectively, at frequencies of $8 \cdot 10^{-4}$ and $3.1 \cdot 10^{-3}$ Hz, characterize changes in the signal level with a period of 20.8 and 5.3 min. The position of peak C in relation to the set of local spectral densities of fluctuations in the mean-minute values of the signal level is sufficiently stable, but its value and width vary substantially in relation to the length of the yearly realization. The position of peak D, on the contrary, is unstable.

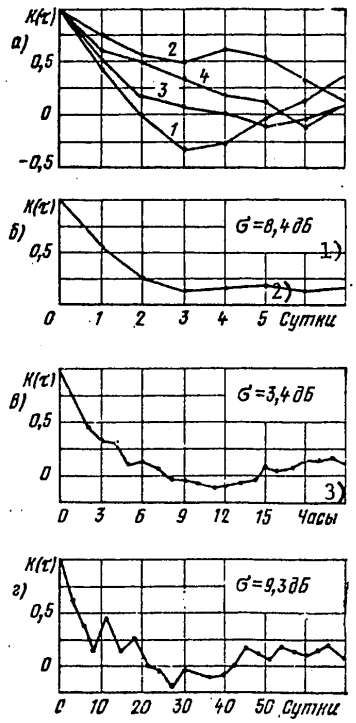

Figure 2.

Key:
1. dB
2. 24-h periods
3. hours

A physical interpretation of these peaks is difficult in view of the little investigation of the spectral properties of meteorological parameters, in particular, the refractive index [9]. The expected spectral density peak at a frequency of $3.22 \cdot 10^{-8}$, reflecting seasonal variations in the signal level, was not reproduced because of the limited nature of the length of the measured realization.

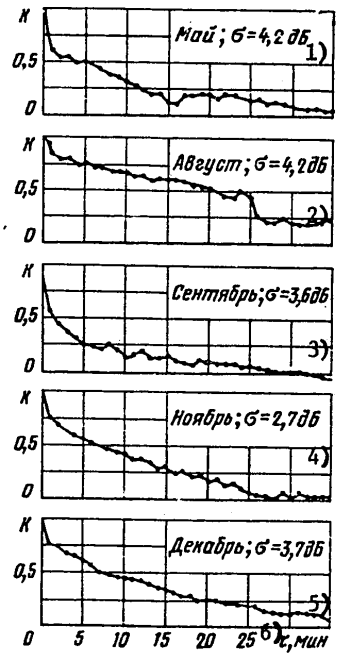

Figure 3.

Key:

1. May, dB
2. August
3. September
4. November
5. December
6. τ, min

The dependence of the spectral density on frequency (fig 1) is approximated well by power function $G(f) = f^{-7/5}$. The absolute value of the exponent here proved to be somewhat lower than the similar parameter for approximation of the spectral density of time-dependent fluctuations in the refractive index [9]. However, the spectra analyzed in [9] were arrived at by processing only individual realizations and characterize intermittent fluctuations in the refractive index to frequencies not lower than $4.2 \cdot 10^{-3}$ Hz.

Let us note that the spectral form for representing the results of measurements of the signal level makes it possible to estimate quantitatively the strength of fluctuations in the signal level in any frequency band of interest to the investigator.

In conclusion the author wishes to express his thanks to G.A. Kalinov and A.A. Kashkan for their helpful discussions of this article's material and for their assistance in computations and in processing experimental data.

Bibliography

1. Vvedenskiy, B.A. et al., eds. "Dal'neye troposfernoye rasprostraneniye UKV" [Long-Range Tropospheric Propagation of Ultrashort Waves], Moscow Sovetskoye Radio, 1965.

2. Tsvetkov, E.I. "Nestatsionarnyye sluchaynyye protsessy i ikh analiz" [Nonstationary Random Processes and Their Analysis], Moscow, Energiya, 1973.

3. Gribanov, Yu.I. and Mal'kov, V.L. "Spektral'nyy analiz sluchaynykh protsessov" [Spectrum Analysis of Random Processes], Moscow, Energiya, 1974.

4. Bendat, Dzh. and Prisol, A. "Izmereniye i analiz sluchaynykh protsessov" [Measurement and Analysis of Random Processes], translated from English, Moscow, Mir, 1974.

5. Shur, A.A. "Kharakteristiki signala na troposfernykh radioliniyakh" [Characteristics of a Signal in Tropospheric Radio Lines], Moscow, Svyaz', 1972.

6. Khromov, S.P. and Mamontova, L.I. "Meteorologicheskiy slovar'" [Meteorological Dictionary], Leningrad, Gidrometeoizdat, 1974.

7. Vollerner, N.F. "Apparaturnyy spektral'nyy analiz signalov" [Instrument-Assisted Spectrum Analysis of Signals], Moscow, Sovetskoye Radio, 1977.

8. Geranin, V.A. "Spectral Representation of Nonstationary Random Processes" in "Trudy IV Vsesoyuznoy shkoly-seminara po statisticheskoy gidroakustike" [Proceedings of the Fourth All-Union Training Seminar on Statistical Hydroacoustics], Novosibirsk, USSR Academy of Sciences Siberian Division Institute of Mathematics, 1973.

9. Kazakov, L.Ya. and Lomakin, A.N. "Neodnorodnosti koeffitsienta prelomleniya vozdukha v troposfere" [Inhomogeneities of the Refractive Index of Air in the Troposphere], Moscow, Nauka, 1976.

10. Korneyev, I.L. et al. "Variability of the Mean Level of an Ultrashort Wave Signal in Long-Range Tropospheric Propagation Over the Ocean," ELEKTROSVYAZ', No 1, 1979.

[62-8831]
8831
CSO: 1860

UDC 621.371:621.396.96

DEPOLARIZATION OF RADIO WAVES IN SCATTERING ON VEGETATIVE SOIL

Moscow RADIOTEKHNIKA in Russian No 10, 1979 pp 24-30 manuscript received 14 Dec 78

[Article by A.S. Skryabin]

[Text] Introduction

In recent years a considerable amount of studies have been devoted to analyzing the polarization properties of radio waves [1-4, etc.]. However, the question of the depolarization of radio waves in scattering on actual terrestrial soil has remained open, although it is a decisive question in many practical problems in utilizing their properties. Below a theoretical and experimental investigation is made of the depolarization of radio waves in scattering on vegetative soil (a forest) and an estimate is made of the relative influence of various factors on the amount of depolarization. Discussed is a radar case for a sighting angle relative to the normal line to the mid-level of the base. As demonstrated by the experimental investigations in [5,6], vegetative soil causes the greatest depolarization of radio waves. For theoretical investigations scatterers of this source can be represented in the form of a three-dimensional structure consisting of disks and linear reflectors.

In the scattering of radio waves on vegetative soil, depolarization is caused chiefly by the edge wave, anisotropy of the reflector and multiple scattering. By anisotropy will be meant a difference in the shape of the reflector from a regular spherical. If it differs in one coordinate, then the reflector has the shape of an oblate ellipsoid, changing at its end into a circular disk. For plane reflectors there occurs a difference in two coordinates, and the reflector can change shape from a round disk to an elliptical one, changing at its limit into a linear reflector.

Theory

Let us investigate the depolarization of radio waves in scattering in a three-dimensional structure consisting of circular ideally conducting disks and linear reflectors. Let us consider the case of $ka < 1$ and

ka > 1 (where a is the radius of the disk or half the length of the linear reflector and $k = 2\pi/\lambda$ is the wave number).

For a disk the case of ka < 1 is investigated on the basis of Eggimann's study [7] and the case of ka > 1 by the method of edge waves [8]. The geometry of scattering is represented in fig 1. Axis Z_0 is perpendicular to the surface of the ground and axis Z to the plane of the disk.

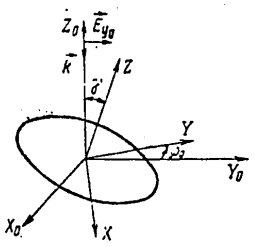

Figure 1.

For the purpose of estimating the amount of depolarization we employ the depolarization coefficient,

$$D(\varphi_0, \gamma, ka) = \left(\frac{|\dot{E}^{\perp}(\varphi_0, \gamma, ka)|^2}{|\dot{E}^{\parallel}(\varphi_0, \gamma, ka)|^2}\right)^{\frac{1}{2}},$$

where $\dot{E}^{\perp}(\phi_0,\gamma,ka)$ and $\dot{E}^{\parallel}(\phi_0,\gamma,ka)$ are components polarized orthogonally to and parallel with, respectively, the radiated wave.

First were obtained dependences of the depolarization coefficient on aspects ϕ_0 and γ and dimension ka for the case of scattering on a single reflector. Then was computed the mean value of the depolarization coefficient, $|\bar{G}|$, for an ensemble of identical disks oriented with equal probability. Let us assume that the disks occupy a space with dimensions much greater than λ and are widely spaced so that it is possible to disregard their mutual influence (shading and multiple scattering). Since the signals from individual scatterers are put together as incoherent signals, the equation for the mean value of the depolarization coefficient has the form

$$\overline{D}(\varphi_0, \gamma) = \left(\frac{\overline{\left[\dot{E}^{\perp}(\varphi_0, \gamma)\right]^2}}{\overline{\left[\dot{E}^{\parallel}(\varphi_0, \gamma)\right]^2}}\right)^{\frac{1}{2}} = \left(\frac{\int_{\varphi_0=0}^{2\pi}\int_{\gamma_1}^{\gamma_2}\left[\dot{E}^{\perp}(\varphi_0, \gamma)\right]^2 \sin\gamma d\varphi_0 d\gamma}{\int_{\varphi_0=0}^{2\pi}\int_{\gamma_1}^{\gamma_2}\left[\dot{E}^{\parallel}(\varphi_0, \gamma)\right]^2 \sin\gamma d\varphi_0 d\gamma}\right)^{\frac{1}{2}} = \left(\frac{A}{B}\right)^{\frac{1}{2}}. \quad (1)$$

An experiment has demonstrated that the range of the aspects of reflectors (leaves, needles and branches) equals $\phi_0 = 0$ to 2π and $\gamma = \pi/2$; consequently, the integration limits in equation (1), in calculating the mean value of the coefficient of depolarization from a forest, must be taken as from 0 to 2π for ϕ_0 and from 0 to $\pi/2$ for γ . For a low-frequency (LF) approximation, the integrals for ϕ_0 and γ are reduced to tabular and the solution is arrived at analytically. For a high-frequency approximation, the integral for ϕ_0 is reduced to tabular and integration for γ is carried out on an M-220 computer. The results of calculations are presented in fig 2, in which are illustrated dependences of $|\overline{D}| = f(ka)$ for 1) $\gamma = 0$ to 90° and 2) $\gamma = 0$ to 20° (the latter case is characteristic of dry land in the absence of vegetation and of an ocean in the absence of whitecaps). The preliminary results arrived at by means of a model of an ensemble of randomly oriented identical disks are given in [9].

Let us evaluate the accuracy of the theoretical procedure. Matson [10], having investigated the error of the Eggimann method as compared with a strict solution, demonstrated that with $ka = 0.5$ the discrepancy equals 0.1 dB. With $ka = 1$ can be expected an increase in the discrepancy to a few tenths of a decibel. An estimate of the error of the high-frequency (HF) approximation was made by M.G. Belkina [11], T.Ya. Ufimtsev [8] and others for $ka = 5$, 3 and 1 . It equals fractions of a decibel and has a different sign with different sighting angles. Therefore in averaging over the entire range of angles this error is compensated to a considerable extent. With $ka \gg 1$ the error of the theoretical procedure equals less than 0.1 dB.

In the vicinity of point $ka = 1$ the graphs of the LF and HF approximations are conjugated smoothly.

Let us estimate the error of experimental methods. In determining the effective areas of scattering (EPR's) of bodies of simple geometrical shape, the accuracy is rarely higher than 30 percent (about 1 dB) [12]. The error of absolute methods of measuring the EPR's of terrestrial soil

equals 3 to 5 dB, and in calibrating with reference to a standard reflector it is reduced to 2 to 3 dB. In comparative measurements of the depolarization factor, $|\bar{D}|$, by the compensation method the error is about 1 dB.

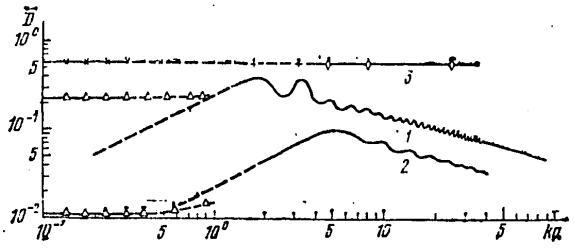

Figure 2.

Since the error of theoretical methods with any ka is considerably lower than the error of experimental methods, then the theoretical procedure is applicable with a degree of precision sufficient for practice with any ratios of the dimensions of reflectors and the length of the radio wave.

The mean value of the depolarization coefficient for an ensemble of linear reflectors oriented with equal probability has been computed by disregarding mutual shading and multiple scattering. The geometry of scattering for a single linear reflector is illustrated in fig 3.

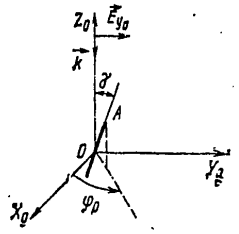

Figure 3.

For a low-frequency approximation the expression for the mean value of the depolarization coefficient for all orientations of linear reflectors has the form [13]

$$\overline{D}_{1,2}^{-1}(\bar{\varphi}_0, \gamma) = \left(\frac{\overline{\left[\dot{E}^{\perp}(\varphi_0, \gamma)\right]^2}}{\overline{\left[\dot{E}^{\parallel}(\varphi_0, \gamma)\right]^2}}\right)^{\frac{1}{2}} = \left(\frac{\int_{\varphi_0=0}^{2\pi} \sin^2\varphi_0 \cos^2\varphi_0 d\varphi_0 \int_{\gamma=0}^{\pi/2} \sin^4\gamma d\gamma}{\int_{\varphi_0=0}^{2\pi} \cos^4\varphi_0 d\varphi_0 \int_{\gamma=0}^{\pi/2} \sin^3\gamma d\gamma}\right) =$$

$$= \frac{1}{\sqrt{3}} \approx 0{,}58. \qquad (2)$$

Consideration of the HF approximation, when the length of the reflector equals $\ell >> \lambda$ and its diameter equals $\phi << \lambda$ results in the same final results for the mean value of the depolarization coefficient as in the LF approximation (equation (2)). The results obtained for linear reflectors are presented in fig 2 (cf. graph 3, where the X's represent the low-frequency approximation, the diamonds represent the high-frequency approximation, and the plusses the results [16]).

According to fig 2 (curve 3) $|\overline{D}|_1 = 0.58$ and does not depend on ka and γ. This was arrived at as the result of the fact that the idealized case was considered, when the diameter of the linear reflector is much less than its length, $\phi << \ell$ and $\phi << \lambda$, in disregarding the influence of cross currents and the end surfaces. In taking into account the finite value of the cross section and the influence of end surfaces, there should be evidenced a dependence of $|\overline{D}|$ on γ and ka and with an increase in ka should be observed a drop in the value of $|\overline{D}|$. According to fig 2 (curves 1 and 2) the magnitude of the mean value of the depolarization coefficient, $|\overline{D}|_d$, in scattering in a cluster of circular disks, depends on ka and γ: With $ka < 1$ this dependence is slight, and with $ka > 1$ it is of an oscillating decrement nature.

The above makes it possible to estimate the relative influence of the edge wave and of the anisotropy of the reflector on the value of the depolarization coefficient for the most typical cases as a function of the shape of the reflector, the range of aspects and the dimensions.

An increase in anisotropy--a change in shape from a disk to a linear reflector--causes an increase in the depolarization coefficient during scattering in this reflector and a change in the nature of the dependence of $|\overline{D}|$ on ka and ϕ_0 and γ.

In the case of a cluster of reflectors situated perpendicularly to the incident field ($\gamma = 0$ in fig 1 and $\gamma = 90°$ in fig 3) and oriented with

equal probability relative to an angle of turn, ϕ_0, from 0 to 2π, depolarization is determined totally by the anisotropy of the reflector. For a cluster of disks $|\bar{D}_d| = 0$ for any ka and for a cluster of linear reflectors $|\bar{D}_l| = 0.58$ for any ka.

In scattering in a cluster of reflectors distributed with equal probability over all orientations, the magnitude of the mean value of the depolarization coefficient is determined by the edge wave and the anisotropy of the reflector. According to fig 2 (curve 1) the value of $|\bar{D}_d|$ caused by an edge wave equals 0.23 in the LF region and $|\bar{D}_d| \sim (ka)^{1/2}$ in the HF region. From a comparison of graph 1 and 3 it follows that an increase in the anisotropy of the reflector (transition from a disk to a linear reflector) increases the mean value of the depolarization coefficient from 0.23 to 0.58 in the LF region and by $\sqrt{ka}$ in the HF region.

Let us consider the more common case when the ensemble consists of disks of different sizes and let us determine the mean value of the depolarization coefficient of radio waves in this case. For this it is necessary in the numerator and denominator of equation (1) to integrate also for ka, taking into account the distribution density of this parameter,

$$\bar{D}_{\text{в.л}}(\varphi_0, \gamma, ka) = \left(\frac{\overline{\left|\dot{E}^{\perp}(\varphi_0, \gamma, ka)\right|^2}}{\overline{\left|\dot{E}^{\parallel}(\varphi_0, \gamma, ka)\right|^2}}\right)^{\frac{1}{2}} =$$

$$= \left(\frac{\int_{ka_1}^{ka_2}\int_{\varphi_0=0}^{2\pi}\int_{\gamma=0}^{\pi/2}\left[\dot{E}^{\perp}(\varphi_0, \gamma, ka)\right]^2 W(ka)\sin\gamma\, d\varphi_0\, d\gamma\, d(ka)}{\int_{ka_1}^{ka_2}\int_{\varphi_0=0}^{2\pi}\int_{\gamma=0}^{\pi/2}\left[\dot{E}^{\parallel}(\varphi_0, \gamma, ka)\right]^2 W(ka)\sin\gamma\, d\varphi_0\, d\gamma\, d(ka)}\right)^{\frac{1}{2}} =$$

$$= \left(\frac{\int_{ka_1}^{ka_2} AW(ka)\, d(ka)}{\int_{ka_1}^{ka_2} BW(ka)\, d(ka)}\right)^{\frac{1}{2}}. \qquad (3)$$

The distributions of the dimensions of reflectors in real terrestrial soil are rather complex: In fig 4a is given the distribution of the dimensions of the leaves of a birch tree, in fig 4b of an aspen and in fig 4c of an oak. These curves were obtained experimentally for the woods in the Moscow region in August, when the growth of leaves has stopped. Along the X axis are plotted numerical values of the length of a leaf without the stem, ℓ, expressed in centimeters and in values of ka for wavelengths of 3 and 36 cm, at which the experiment was performed [6].

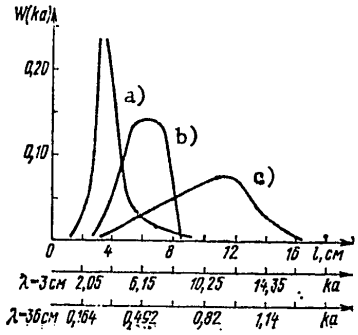

Figure 4.

It is a complicated affair to arrive at a mathematical expression for the distribution function, in view of which a numerical integration was performed in terms of ka . In equation (3) the numerator and denominator under the square root sign are proportional to the EPR's of the ensemble of reflectors for orthogonally and parallel polarized components. Since these values are of independent interest, it is a good idea to compute them and compare them with the experimental data [4,6].

As an example was computed the matrix of EPR's of a birch forest.

For waves with $\lambda = 3$ cm , $ka > 1$, and consequently it is necessary to use the equations of the HF approximation:

$$\sigma^{\perp}_{a.в} = \frac{\pi k^2}{2} \sum_{l=1}^{r} a_l^4 A_в W(ka) n, \qquad \sigma^{\parallel}_{a.в} = \frac{\pi k^2}{2} \sum_{l=1}^{r} a_l^4 B_в W(ka) n,$$

where $\sigma^{\perp}_{a.v}$ and $\sigma^{\parallel}_{a.v}$ are the effective scattering areas of the ensemble of reflectors for the HF approximation, A_v and B_v are the numerator and denominator under the square root in equation (1) for the HF approximation, n is the number of reflectors in the ensemble and r is the number of division intervals for ka .

For waves with $\lambda = 36$ cm , $ka < 1$; therefore the equations of the LF approximation are valid:

$$\sigma^{\perp}_{a.н} = \frac{4k^4}{135\pi^2}\sum_{i=1}^{r} a_i^6 A_н W'(ka)\, n, \qquad \sigma^{\parallel}_{a.н} = \frac{7\Gamma k^4}{135\pi^2}\sum_{i=1}^{r} a_i^6 B_н W(ka)\, n,$$

where $\sigma^{\perp}_{a.n}$ and $\sigma^{\parallel}_{a.n}$ are the effective scattering areas of the ensemble of reflectors for the LF approximation and A_n and B_n are the numerator and denominator under the square root in equation (1) for the LF approximation.

In the calcuations it was assumed that in the spot irradiated there is a single adult birch about 15 m high with a top diameter of approximately 15 m and with $n = 10^4$. The results of calculations of the EPR of the top of a birch for parallel polarized component $\sigma^{\parallel}$ are given in the fourth column of table 1, and for the orthogonally polarized component, $\sigma^{\perp}$, in the second column. In the third and fifth columns are given specific EPR's (UEPR's), in the sixth experimental values of UEPR's from [4] and in the seventh column, calculated values of $\left|\frac{1-\bar{l}}{D}\right|$.

Table 1.

1	2	3	4	5	6	7
λ, см	$\sigma^{\perp}$, м²	$\sigma^{\perp}_0$	$\sigma^{\parallel}$ м²	$\sigma^{\parallel}_0$	$\sigma^{\parallel}_0$ [4]	$\left\|\frac{1-\bar{l}}{D}\right\|$
3	1,24	0,027	27,6	0,6	0,1—0,8	0,212
36	$9\cdot10^{-5}$	$1{,}9\cdot10^{-6}$	$1{,}7\cdot10^{-3}$	$3{,}8\cdot10^{-5}$	0,5—2	0,22

The calculated values of UEPR's for a wave with $\lambda = 3$ cm are of the same order of magnitude as the experimental from [4]. This demonstrates that in the scattering of waves of this range on a forested area the major influence is exerted by the leaves of the trees.

For a wave with $\lambda = 36$ cm the calculated values of UEPR's are lower than the experimental from [4] by approximately four orders of magnitude, i.e., the leaf cover practically does not play a role in the process of the scattering of radio waves of the 36 cm band on a forested area. A decisive role in the process of scattering of radio waves with $\lambda = 36$ cm is played by the earth base. The results of experiments on the attenuation of radio waves in passing through a forested area [14] also confirm that vegetation causes relatively slight attenuation of radio waves with $\lambda = 36$ cm.

Experiment

Measurements were made of the mean values of depolarization coefficients in scattering on a forested area for a sighting angle along the normal line to the ground surface. The experiment itself and the apparatus were described in [6]; measurement results are given in secs 1 and 2 of table 2, where S_D is the root-mean-square deviation in the depolarization coefficient and δ (percent) is the root-mean-square value of the total instrument error of the measurements.

Table 2.

№ п/п	1) Тип отражателя	λ, см	$\overline{\lvert D \rvert}$	S_D	δ, %	2) Источник	
1	3) Лес смешанный с листвой	3	0,86	0,14	9	[6]	Экспериментальные данные
		3	0,8	0,35	21	[15]	
2	Лес смешанный с частично опавшей листвой 4)	3	0,37	0,06	9	[6]	8)
		36	0,08	0,008	17	[6]	
3	5) Облако равновероятно ориентированных линейных отражателей	$a \ll \lambda$	0,58			[13]	Теоретические результаты 9)
		$a = \frac{\lambda}{4} \div \frac{\lambda}{2}$	0,58	0,01		[16]	
		$a \gg \lambda$	0,58				
4	Облако равновероятно ориентированных листьев березы 6)	3	0,212				
		36	0,22				
5	Облако из листьев березы и хвои 7)	3	0,40				
		36	0,39				

Key:

1. Type of reflector
2. Source
3. Mixed forest with foliage
4. Mixed forest with partly shed foliage
5. Cluster of equally probably oriented linear reflectors

[Key continued on following page]

6. Cluster of equally probably oriented birch leaves
7. Cluster of birch leaves and coniferous needles
8. Experimental data
9. Theoretical results

In the last column are indicated the method of arriving at the results and the bibliographic source.

Discussion of Results

In the theoretical section were computed the values of the depolarization coefficient caused by the edge wave and anisotropy of the reflector. We evaluate the relative influence on depolarization of multiple scattering by comparing the experimental and theoretical results. A comparison of experimental results for the depolarization of radio waves of the 3 cm band (secs 1 and 2 of table 2) demonstrates that a mixed forest with foliage causes 2.3-fold greater depolarization than a mixed forest with partly shed foliage, which can be explained by the influence of multiple scattering.

In sec 5 of table 2 are given the results of theoretical calculations of the mean value of the depolarization coefficient of radio waves of the 3 cm band in scattering on a cluster of equally probably oriented reflectors, when at the irradiated spot are found birch leaves and coniferous needles (linear reflectors), whereby the levels of parallel polarized components reflected from leaves and needles are identical. Depolarization in this case is caused by the edge wave and anisotropy of the reflector. The mean value of the depolarization coefficient equals 0.4, which agrees well with the experimental magnitude of the mean value of the depolarization coefficient for a mixed forest with partly shed foliage.

A comparison of the experimental results for $\lambda = 3$ cm (sec 1 and 2 of table 2) and the theoretical results for a three-dimensional structure of equally probably oriented reflectors (sec 5) demonstrates that multiple scattering begins to exert an influence on the amount of depolarization with an increase in the density of the forested area and practically can raise the value of the depolarization coefficient 2.3-fold.

The experimental and theoretical results with $\lambda = 36$ cm for a cluster of equally probably oriented reflectors differ substantially. (The experimental magnitude of the mean value of the depolarization coefficient is 12 to 14 dB lower than the theoretical.) This is caused by the fact that the leaf cover practically does not play an important role in the process of scattering of radio waves with $\lambda = 36$ cm in a forested area. The decisive role in the process of the scattering of radio waves of this band is played by the ground base; therefore, if in the theoretical equations are substituted the geometrical parameters not of the three-dimensional structure but of the base ($\gamma = 0$ to 20°), corresponding to curve

2 in fig 2, it is possible to obtain better agreement of the theoretical and experimental magnitudes of the mean value of the depolarization coefficient.

Bibliography

1. Kanareykin, D.B., Pavlov, N.F. and Potekhin, V.A. "Polyarizatsiya radiolokatsionnykh signalov" [Polarization of Radar Signals], Moscow, Sovetskoye Radio, 1966.

2. Beckmann, P. "Depolarization of Electromagnetic Waves," Colorado, The Golem Press, 1968.

3. Pozdnyak, S.I. and Melitskiy, V.A. "Vvedeniye v statisticheskuyu teoriyu polyarizatsii radiovoln" [Introduction to the Statistical Theory of the Polarization of Radio Waves], Moscow, Sovetskoye Radio, 1974.

4. Zubkovich, S.G. "Statisticheskiye kharakteristiki radiosignalov, otrazhennykh ot zemnoy poverkhnosti" [Statistical Characteristics of Radio Signals Reflected from the Surface of Earth], Moscow, Sovetskoye Radio, 1968.

5. Skryabin, A.S. "Tezisy XXV Vsesoyuznoy nauchnoy sessii NTORES imeni A.S. Popova" [Theses of the 25th All-Union Scientific Session of the Scientific and Technical Society of Radio Engineering and Telecommunications imeni A.S. Popov], Moscow, Sovetskoye Radio, 1969.

6. Skryabin, A.S. RADIOTEKHNIKA, Vol 28, No 1, 1973.

7. Eggimann, W.H. TRANS. IRE, Vol MTT-9, No 5, 1961.

8. Ufimtsev, P.Ya. "Metod krayevykh voln v fizicheskoy teorii difraktsii" [Method of Edge Waves in the Physical Theory of Diffraction], Moscow, Sovetskoye Radio, 1962.

9. Kovalev, V.F., Kormilitsin, B.T., Skryabin, A.S. and Tokar', V.G. "VI Vsesoyuznyy simpozium po difraktsii i rasprostraneniyu voln" [Sixth All-Union Symposium on Wave Diffraction and Propagation], Book 1, Yerevan, 1973.

10. Matson, J.R. TRANS. IEEE, Vol AP-19, No 1, 1971.

11. Belkina, M.G. Article in book "Difraktsiya elektromagnitnykh voln na nekotorykh telakh vrashcheniya" [Diffraction of Electromagnetic Waves on Some Solids of Revolution], Moscow, Sovetskoye Radio, 1957.

12. Shtager, Ye.A. and Chayevskiy, Ye.V. "Rasseyaniye voln na telakh slozhnoy formy" [Scattering of Waves on Bodies of Complex Shape], Moscow, Sovetskoye Radio, 1974.

13. Long, M.W. TRANS. IEEE, Vol AP-13, No 5, 1965.

14. Sekston, D. and Leyn, D. "Voprosy radiolokatsionnoy tekhniki" [Questions of Radar Technology], No 5 (29), 1955.

15. Campball, J.P. "Proceedings of the National Conference on Aeronautical Electronics," 1958.

16. Mack, C.L. and Reiffen, B. IEPIEEE, Vol 52, No 5, 1964.

[59-8831]

CSO: 1860
8831

UDC 621.371.247:551.5

APPROXIMATE DETERMINATION OF STATISTICAL DISTRIBUTIONS OF INTENSITY OF RAINFALL

Moscow ELEKTROSVYAZ' in Russian No 10, 1979 pp 49-51 manuscript received 27 Mar 79

[Article by Ye.A. Larin]

[Text] Introduction

In the process of the development of radio relay and satellite communications equipment a trend has been distinctly traced in the mastery of higher and higher frequency bands. Able to be fulfilled in practice at the present time is the objective of creating in the shortwave end of the SHF and the longwave end of the EHF wavebands radio relay and satellite communications systems which will make it possible considerably to increase the volume of information transmitted and to carry out its transmission in digital form.

The attenuation of radio waves in rain represents here an important obstacle. For the purpose of determining this attenuation and consequently for estimating the reliability of these communications systems, it is necessary to have information on the probability of the falling of rain of different intensity in a specific month of the warm time of the year for different climate regions. Obtaining this information by processing the data of meteorological measurements involves great difficulties, and for some areas is entirely impossible because of the lack of observations. In some instances the amount of data to be processed is reduced, i.e., data are processed on rainfall which has the greatest influence on the propagation of radio waves in these bands.

The establishment quantitatively of a criterion for selecting observations for processing is not simple in view of the diversity of practical problems. The criterion sometimes used [1], according to which for the purpose of plotting statistical distributions data are sampled of observations for rain with a total rainfall of 10 mm and more, has been occasioned chiefly by the existence of such published data for the majority of regions of the country. It is obvious that statistical distributions obtained in this manner indicate somewhat too low values of the probability of exceeding

a specific intensity of rainfall, as compared with distributions which take into account all rainfall. Moreover, the degree of this underestimate will depend on the climatic region and the time of year.

In order to avoid errors of this nature it is necessary to have knowledge of statistical distributions of intensity for all rainfall. In solving this problem indirect methods of estimating have greater possibilities than the method of directly processing meteorological data. One of these methods is suggested in this article. For its substantiation have been employed the following meteorological data: the results of a 10-year period of observation of the variation in the intensity of rainfall with a total rainfall of 5 mm and more for different climate regions of the country, and data on the duration of rainfall for a month [2].

General Expression for the Statistical Distribution of the Intensity of Rainfall

As a result of analyzing a great number of monthly empirical statistical distributions of the intensity of rainfall, plotted from meteorological data for many years, it was established that these distributions can be approximated with a degree of precision satisfactory for practice, by the following general equation:

$$F(I) = c \exp\left[-(I/\beta)^{\gamma}\right], \tag{1}$$

where I is the intensity of rainfall; $F(I)$ is the statistical distribution of the intensity of rainfall for each value of I, equal to the probability of the event that the intensity of rainfall for a month will exceed this value, and α, β, and γ are parameters.

Parameter α represents the probability of rainfall at a specific point. The mean relative duration of rainfall for a month [2] serves as its estimate.

For the purpose of finding estimates of parameters β and γ, first, based on the data of observations over many years, were plotted statistical distributions of the intensity of rainfall for each month from May through September for regions of the country having considerable climate differences. Then, from these distributions were calculated the mean intensity of the rain while it fell and the variance in intensity during this same period. It was shown that these values on average are related by the equation

$$D = 6\bar{I}, \tag{2}$$

where $\bar{I}$ is the average intensity of rainfall in mm/h and D is the variance in the intensity of rainfall in mm^2/h^2. Dependence (2) is shown

in fig 1 by the solid line. Attention is drawn by the relatively not too great variance in points in relation to the mean line, in spite of the fact that they indicate ratios of $D/\overline{I}^2$ for different climate regions and months of the year differing in shower activity.

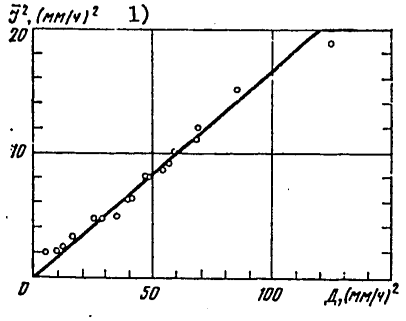

Figure 1.

Key:
1. $(\text{mm/h})^2$

This fact testifies to the steadiness of the dependence found. However, it is not convenient to use it, since it was derived on the basis of data for rain with a total rainfall of 5 mm and more. In order to obtain a dependence similar to (2) but characterizing the entire rainfall at a certain observation point, we assume that the statistical distribution of intensity for all the rain and for rain with a total rainfall of 5 mm and more have the same form, (1). With very high intensity (60 mm/h and more) these distributions practically agree, since high intensity is most probable in rain with a total rainfall of 5 mm and more. An analysis of observation data from several meteorological stations containing the behavior of all rainfall has confirmed this assumption. On its basis, taking into account the assumption regarding the shape of the statistical distribution of intensity for all rainfall and data on the duration and mean intensity of rainfall [2], calculations were performed which have made it possible to obtain the following relationship:

$$D_0 = 11 I_0^2, \tag{3}$$

where I_0 is the mean value of the intensity of all rainfall in mm/h and D_0 is the variance in the intensity of all rainfall in mm^2/h^2.

It is possible to demonstrate [3] that if a direct proportional relationship exists between the square of the mean value and the variance in the random value obeying law (1), then parameter γ is a constant value. Utilizing the table in [3] and bearing (3) in mind, we get $\gamma = 0.39$.

The mean intensity of rainfall is related to parameters β and γ by the equation

$$I_0 = \beta K(\gamma), \tag{4}$$

where $K(\gamma)$ is a tabulated function [3]. With $\gamma = 0.39$, function $K(\gamma) = 3.65$. Substituting (4) in (1), with $\gamma = 0.39$ we get the final equation for calculating statistical distributions of the intensity of rainfall at the observation point:

$$F(I) = \alpha \exp\left[-1{,}66\,(I/I_0)^{0{,}39}\right]. \tag{5}$$

For the purpose of simplifying calculations, in fig 2 is given the dependence

$$F_1(I) = \exp\left[-1{,}66\,(I/I_0)^{0{,}39}\right],$$

by means of which it is possible easily to plot F(I) for points which are multiples of I_0 , and in table 1 are given values of estimates of parameters α and I_0 for different meteorological stations in the country.

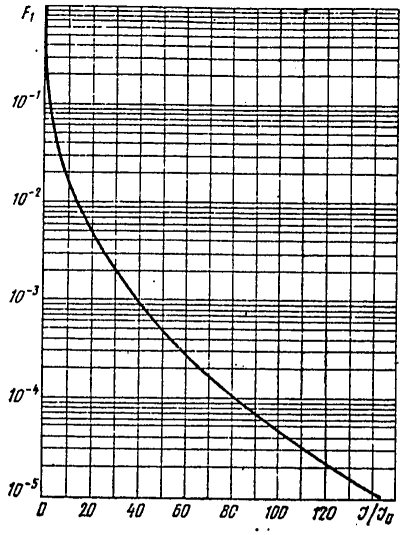

Figure 2.

Table 1.

1) Город, где расположена метеостанция	3) Значение оценок вероятности выпадения дождя α и его средней интенсивности I_0 по месяцам									
	4) май		5) июнь		6) июль		7) август		8) сентябрь	
	α	I_0	α	I_0	α	I_0	α	I_0	α	I_0
Архангельск 2)	0,13	0,41	0,10	0,81	0,08	1,04	0,10	0,82	0,15	0,57
Ленинград	0,09	0,63	0,08	1,02	0,07	1,17	0,08	1,34	0,11	0,75
Вильнюс	0,09	0,74	0,08	1,23	0,08	1,47	0,06	1,47	0,09	0,85
Москва	0,09	0,71	0,07	1,30	0,06	1,77	0,08	1,21	0,09	0,88
Минск	0,08	0,97	0,06	1,75	0,07	1,61	0,07	1,57	0,09	0,86
Курск	0,08	0,94	0,06	1,66	0,07	1,49	0,07	1,17	0,07	0,83
Львов	0,12	0,72	0,11	1,12	0,09	1,41	0,10	1,11	0,10	0,72
Ужгород	0,08	1,04	0,10	1,26	0,07	1,49	0,07	1,51	0,06	1,34
Донецк	0,06	1,09	0,06	1,43	0,04	2,08	0,04	1,64	0,04	1,00
Волгоград	0,05	0,81	0,03	1,48	0,03	1,34	0,03	1,21	0,03	1,07
Ростов-на-Дону	0,04	1,44	0,04	2,11	0,03	2,28	0,03	1,61	0,03	1,48
Батуми	0,13	0,88	0,09	2,34	0,10	2,33	0,12	2,77	0,15	2,76
Тбилиси	0,11	1,05	0,09	1,11	0,05	1,29	0,05	1,00	0,08	0,73
Павлодар	0,04	0,74	0,05	0,86	0,05	0,94	0,03	1,47	0,04	0,63
Караганда	0,07	0,54	0,06	0,97	0,05	1,18	0,04	0,93	0,05	0,58
Омск	0,06	0,67	0,06	1,15	0,07	1,30	0,06	1,03	0,07	0,63
Томск	0,10	0,59	0,08	1,07	0,05	2,04	0,08	1,17	0,10	0,65
Красноярск	0,11	0,45	0,07	1,05	0,07	1,51	0,08	1,22	0,11	0,57
Улан-Удэ	0,05	0,67	0,06	0,74	0,08	1,15	0,10	0,83	0,06	0,63
Благовещенск	0,08	0,69	0,10	1,30	0,08	2,06	0,09	1,62	0,12	0,84
Магадан	0,14	0,25	0,16	0,37	0,23	0,33	0,17	0,48	0,20	0,51
Владивосток	0,14	0,62	0,23	0,52	0,23	0,56	0,17	1,12	0,09	1,86

Key:

1. City where meteorological station is located
2. Arkhangel'sk, Leningrad, Vil'nyus, Moscow, Minsk, Kursk, L'vov, Uzhgorod, Donetsk, Volgograd, Rostov-na-Donu, Batumi, Tbilisi, Pavlodar, Karaganda, Omsk, Tomsk, Krasnoyarsk, Ulan-Ude, Blagoveshchensk, Magadan, Vladivostok
3. Value of estimates of the probability of rainfall, α, and of its mean intensity, I_0, by month
4. May
5. June
6. July
7. August
8. September

Estimate of Agreement Between Calculated and Empirical Data

In table 2 are given calculated values of the intensity of rainfall for July and empirical values corresponding to them, obtained by processing meteorological data for 10 years. In the calculations were used values of α and I_0 derived from the same meteorological data.

Table 2.

1) Пункт наблюдения	2) Значения статистических распределений интенсивности дождя, мм/ч, превышаемые с вероятностями					
	10^{-3}		10^{-4}		10^{-5}	
	3) Расчет	4) Наблюдение	Расчет	Наблюдение	Расчет	Наблюдение
Подмосковье . 5) . .	14	10	44	40	92	75
Чернигов	14	16	50	54	112	108
Донецк	14	12	50	54	114	120
Центральный район Сальских степей . .	11	14	41	54	101	111
Закарпатье	16	16	51	58	110	156
Уссурийск	15	12	44	39	92	84

Key:

1. Observation point
2. Values of statistical distributions of intensity of rainfall, mm/h, able to be exceeded with a probability of
3. Calculated
4. Observed
5. Moscow region, Chernigov, Donetsk, central region of the Sal Steppes, Transcaucasus, Ussuriysk

It is obvious from table 2 that deviations in the empirical values from the calculated, in terms of the absolute value, on average grow with an increase in the intensity of rainfall and a lowering of probability. However, as the computations demonstrate, the root-mean-square relative deviations are approximately equal for all probability values and equal 15 percent.

It is interesting to note that the same relative deviations are observed between empirical statistical distributions plotted for different 10-year periods of observation for different climate regions of the country. From this it is possible to draw the conclusion that the calculated and empirical statistical distributions of the intensity of rainfall agree in the sense that their deviations do not exceed the variance between empirical distributions characterizing a 10-year period of observation.

This conclusion is valid not only for July but also for other warm months of the year. However, the values of the root-mean-square relative deviations in calculated from empirical values of the intensity of rainfall which can be exceeded with a probability of 10^{-3} to 10^{-5} are increased in the warm spring and fall months, reaching 20 percent.

Conclusion

The method for calculating statistical distributions of the intensity of rainfall was derived on the basis of processing extensive meteorological data on rainfall. It makes it possible to give an estimate of the probability that the intensity of rainfall will exceed a certain specific value. There are no restrictions of any kind on application of the method for obtaining statistical distributions characterizing rainfall for periods of time longer than or less than a month. It is necessary only to substitute in equation (5) values of α and I_0 for the appropriate period of time.

It is possible to demonstrate [4,5,6] that the data obtained, in conjunction with the relationship between the intensity of rainfall and the attenuation of radio waves, is sufficient to calculate the attenuation of radio waves in rain along ground routes of direct visibility and along Earth-space routes.

In writing this article the author was more than once rendered assistance and consultation by associates of the USSR Hydrometeorological Service, for which he expresses to them his deep gratitude.

Bibliography

1. "Inzhenerno-tekhnicheskiy spravochnik po elektrosvyazi. Radioreleynyye linii" [Engineering and Technical Manual for Telecommunications; Radio Relay Lines], Moscow, Svyaz', 1971.

2. Lebedev, A.N. "Prodolzhitel'nost' dozhdey na territorii SSSR" [Duration of Rainfall in the Territory of the USSR], Leningrad, Gidrometeoizdat, 1964.

3. Shor, Ya.B. and Kuz'min, F.I. "Tablitsy dlya analiza i kontrolya nadezhnosti" [Tables for Analyzing and Monitoring Reliability], Moscow, Sovetskoye Radio, 1968.

4. Larin, Ye.A. "Determination of Attenuation of Radio Waves in Rain Along Extended Routes, Based on Statistics on Rainfall" in "Vsesoyuznaya konferentsiya po rasprostraneniyu radiovoln. Tezisy dokladov" [All-Union Conference on Radio Wave Propagation; Theses of Papers], Part 2, Kazan', Kazan' University, 1975.

5. Kalinin, A.I. "Influence of Spatial Nonuniformity of Rainfall on Attenuation of Radio Waves Along Ground Routes," ELEKTROSVYAZ', No 12, 1974.

6. Kalinin, A.I. "Influence of Rain on Attenuation of Radio Waves Along Earth-Satellite Routes," ELEKTROSVYAZ', No 5, 1976.

[62-8831]
CSO: 1860
8831

UDC 621.396:629.12

RESULTS OF TESTS OF THE 'LUCH' DATA TRANSMISSION EQUIPMENT ON VESSELS

Moscow EKSPRESS-INFORMATSIYA, SERIYA PROMYSLOVAYA RADIOELEKTRONNAYA APPARATURA I PODVODNAYA TEKHNIKA in Russian No 11, 1979 pp 1-2

[Article by A.A. Borisovskiy]

[Excerpt] The "Luch" [Beam] domestic data transmission equipment (APD), after the beginning of its series production in 1972, has found wide application in wire channels and trunk radio lines. However, the high requirements for industrial ASU's [automated control systems] with regard to reliability, fidelity and efficiency of data transmission and the lack of marine APD meeting these requirements have made it necessary to study the feasibility of using the "Luch" equipment in radio lines for marine communications.

Accordingly, in 1975 for the first time tests of the "Luch" APD were arranged for on the "Georgiy Ushakov" Scientific Research Weather Vessel (NISP).

In 1977 the USSR Ministry of the Fish Industry Department of Communications and Fish Finding Equipment and the Giprorybflot [State Planning Institute of the Fishing Fleet] Institute organized tests of the "Luch" APD on the "Nakhichevan'" Fish Industry Base (RPB) together with the radio center of the Klaypeda Model Experimental Ocean Fishing Port.

The purpose of these tests was a determination of the feasibility of using the "Luch" APD on vessels, as well as a determination of the key operating and technical characteristics of equipment and duplex radio lines in marine communications of different ranges with modulation rates from 50 to 300 bauds.

In this article are presented generalized data relating to the organization and results of tests, and also conclusions and recommendations on the use of "Luch" APD on vessels of the USSR fishing industry fleet. The material of this article is intended for radio specialists of communications divisions and services, marine radio stations and coastal radio centers and can be useful in the mastery of new equipment and this promising form of communications--data transmission.

Characteristics of Vessels and Structure of Equipment

Key characteristics of vessels and the structure of the equipment taking part in the tests are given in table 1.

Table 1.

Characteristics of vessels and structure of equipment	"Georgiy Ushakov" NISP	"Nakhichevan'" RPB
Displacement, tons	44,000	13,570
Maximum length, m	110	162
Maximum width, m	14.8	21
Height of antennas, m	13.5 to 24	24 to 27
Radio transmitters	"Vyaz-M2," R-64ID	"Brig"
Radio receivers	R-250M2	"Shtil'"
FM add-on module	"Topol'-M"	-
Antennas	UGDSh; inverted-L; 4, 6 and 10 m whips	ShPA-II; inverted-L; 6 m whip
Spacing of antennas, m	5 to 10	5 to 10

[100-8831]

8831
CSO: 1860

UDC 621.372.8.049.75:621.6

MICROWAVE ATTENUATION IN A LINE OF METAL-DIELECTRIC-SEMICONDUCTOR-METAL COMPOSITION

Moscow RADIOTEKHNIKA I ELEKTRONIKA in Russian No 8, 1979
pp 1665-1669

/Article by A. K. Balyko and A. S. Tager/

/Text/ The growth of integrated circuit technology has aroused interest in transmission lines with semiconductor backings. Such lines of metal-dielectric-semiconductor-metal (MDSM) composition or with a Shottky barrier (MSM) (fig. 1) can serve, theoretically, as the basis for creating passive integrated-circuit assemblies as well as active elements with distributed constants (phase inverters, delay lines, traveling-wave LPD's, etc.) [1-8]. However, the technical expedience in applying similar devices essentially depends upon the level of ohmic loss in the elements of such a structure. Insufficient space in the literature has been devoted to the consideration of the losses in MDSM lines. In the majority of works the frequency range below 3 GHz has been studied and only the losses in the semiconductor backing have been taken into consideration. The losses in metallic conductors have been examined only in work [6], but the simplifications made during the analysis led to erroneous results.

This present work examines the characteristics of a distributed MDSM structure in the microwave range with consideration of the losses in the semiconductor and in the metal.

We will examine the propagation of the TM-wave along a line with a two-layered backing depicted in fig. 1.

We will assume that $b \gg d+W$ and that the fringe effects can be ignored. Writing the expressions for the fields in each layer of the structure, the boundary conditions, including the equations for the tangential components of the fields at the interface from $(x=0)$ and the Leontovich conditions for surface con-

ductors ($x=-W$ and $x=d$), we obtain a dispersion equation of the form

(1) $$\beta^2=k_0^2C_{э\phi}L_{э\phi},$$

where

$$L_{э\phi}=\frac{d'-j\dfrac{\omega\varepsilon_0Z_m}{k_0^2}}{1+j\omega\varepsilon_0\varepsilon_2'Z_md'}+\frac{W'-j\dfrac{\omega\varepsilon_0Z_m}{k_0^2}}{1+j\omega\varepsilon_0\varepsilon_1'Z_mW'};$$

$$C_{э\phi}=\left\{\frac{W'}{\varepsilon_1'(1+j\omega\varepsilon_0\varepsilon_1'Z_mW')}+\frac{d'}{\varepsilon_2'(1+j\omega\varepsilon_0\varepsilon_2'Z_md')}\right\}^{-1};$$

$$Z_m=\frac{\mu_0\omega\delta_m}{2}(1+j);\quad k_0^2=\varepsilon_0\mu_0\omega^2;$$

$$W'=\frac{\operatorname{th}(u_1W)}{u_1};\quad d'=\frac{\operatorname{th}(u_2d)}{u_2};$$

$$u_i^2=k_0^2\varepsilon_i'-\beta^2;\quad \varepsilon_i'=\varepsilon_i-\frac{j}{\omega\varepsilon_0\rho_i}\quad (i=1,2).$$

Here $j\beta$ is the propagation constant; ε_i and ρ_i are the relative permittivity and specific resistance of the i-layer (i=1,2); δ_m is the thickness of the skin layer in the metal. In the most interesting practical case of a MDSM structure with $W\ll\lambda_g$, assuming that in (1) $\rho_1\to\infty$, $\rho_2=\rho$, $\varepsilon_1=\varepsilon_2=\varepsilon$, in the frequency range

(2) $$\omega<\omega_*=\frac{1}{d\sqrt{\varepsilon_0\mu_0\varepsilon}},\quad \omega<\omega_S=\frac{\rho}{\mu_0d^2}$$

we obtain

(3) $$\frac{1}{3}(K_1-K_2)^2(\beta d)^4+(\beta d)^2\left[1+K_3(K_1-K_2)+\frac{1}{3}\frac{d_1}{W}\left(\frac{\omega}{\omega_*}\right)^2\right]+$$
$$+\left(\frac{\omega}{\omega_*}\right)^2\left[1+\frac{\delta_m}{W}(1-j)+K_3\frac{d_1}{W}\right]=0.$$

Here

$$K_1=\frac{d}{W}\left(1-j\frac{\omega_D}{\omega}\right)^{-1};\quad \omega_D=(\varepsilon_0\varepsilon\rho)^{-1};$$

$$K_2=\frac{1}{2}\left(\frac{\omega}{\omega_*}\right)^2\left(\frac{\delta_m}{d}\right)\left(1-j\frac{\omega_D}{\omega}\right)(1-j);$$

$$K_3=1+\frac{1}{3}\left(\frac{\omega}{\omega_*}\right)^2\left(1-j\frac{\omega_D}{\omega}\right);$$

$$d_1=d-K_2\left[W+\frac{\delta_m}{2}(1-j)\right].$$

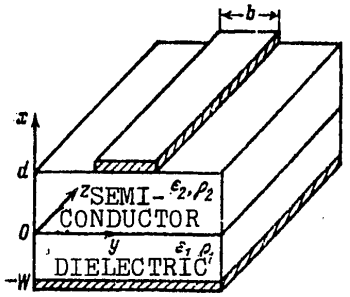

Fig. 1
General view of a MDSM-structured transmission line

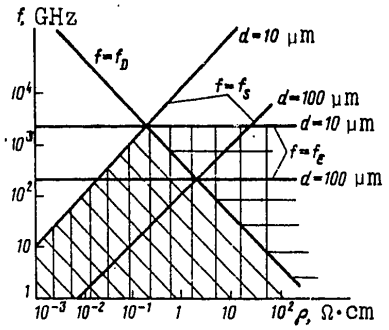

Fig. 2
Plane (ω, ρ)

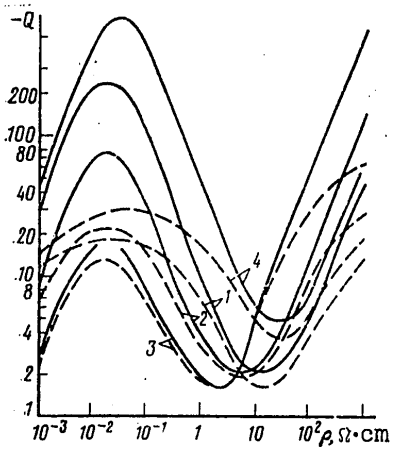

Fig. 3

The function of distributed Q with respect to the specific resistance of the semiconductor ρ when $\delta_m=0$ (solid lines) and $\delta_m\neq0$ (dotted lines) for two thicknesses of dielectric with $\varepsilon=12$: $W=1.0$ μm (1-f=3 GHz, 2-f=10 GHz, 3-f=40 GHz) and $W=5.0$ μm (4-f=3 GHz). $d=10$ μm

The inequalities in (2) on the plane (ω, ρ) (fig. 2) limit the area that is cross-hatched with vertical lines. It surrounds the region of low-velocity waves that is cross-hatched with slanted lines and the region of quasi-TEM-waves cross-hatched with horizontal lines. The borders of these areas depend upon W and d. Thus, equation (3) makes it possible to analyze the characteristics of low-velocity and quasi-TEM-waves, as well as the transition region between them.

We will represent equation (3) in the form

$$\beta = \beta_0 - j\alpha_t = \beta_0 \left(1 - \frac{j}{Q}\right). \tag{4}$$

where $\beta_0 = 2\pi/\lambda_g$ and α_t are the constants of propagation and attenuation in the line; $Q^{-1} = \alpha_t/\beta_0$ is the attenuation of the delayed wave $\lambda_g = \lambda_0/n$.

In fig. 3 a typical function $Q(\rho)$ has been represented. The distinctive shape of the curves is the result of the ρ and $f = \omega/2\pi$ loss component function as it is related to the transverse and longitudinal components of the current in the semiconducting material and the currents in the metallic conductors. The role of each of these factors is much more prominent in the region of low-velocity waves $\omega < (1/2d^2)(W(d+W)/\mu_0 \epsilon \epsilon_0)^{1/2}$, where the solution to equation (3) has the simple form

$$\beta_0 = \omega(\varepsilon\varepsilon_0\mu_0)^{1/2}\left[1 + \frac{d}{W} + \frac{\delta_m}{W}\left(1 + \frac{\omega}{2\omega_s} - \frac{d\omega}{W\omega_D}\right)\right]^{1/2}, \tag{5a}$$

$$\alpha_t = \frac{\beta_0\omega}{2(W+d)}\left[\frac{d}{3\omega_s} + \frac{d(d+W)}{W\omega_D} + \delta_m\left(\frac{1}{\omega} + \frac{1}{2\omega_s} + \frac{d}{W\omega_D}\right)\right]. \tag{5b}$$

The first two terms in the square brackets in expression (5b) characterize, accordingly, the losses brought about by longitudinal and transverse currents in the semiconductor, while the third term characterizes the losses in the metal.* The maximum $Q(\rho)$ on the curves is in the region $\rho = \rho_m = 10^{-3}$-1 $\Omega \cdot$cm. The losses in the conductor noticeably decrease the value of this maximum $Q_m = Q(\rho_m)$; with a backing of set thickness $d+W$ the influence of these losses grows weaker when the frequency increases. In practice, the value of ρ_m in the frequency range of 1-30 GHz does not depend upon the frequency and the losses

* Errors have been made in the simplification of the dispersion equation in [6], as a result of which terms related to the transverse currents in the semiconductor drop out in the final expressions.

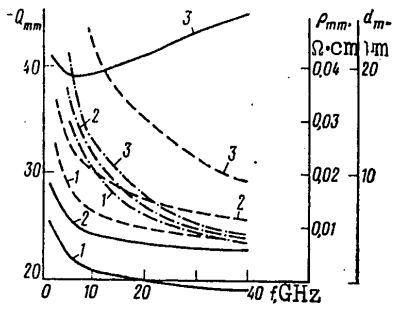

Fig. 4

The function $Q_m(d)$ for two values of thickness of the dielectric: W=1.0 μm (1-f=3 GHz, 2-f=10 Ghz, 3-f=40 GHz) and W=5.0 μm (4-f=3 GHz) when δ_m=0 (solid line) and when $\delta_m \neq 0$ (dotted line). ϵ=12, $\rho=\rho_m$

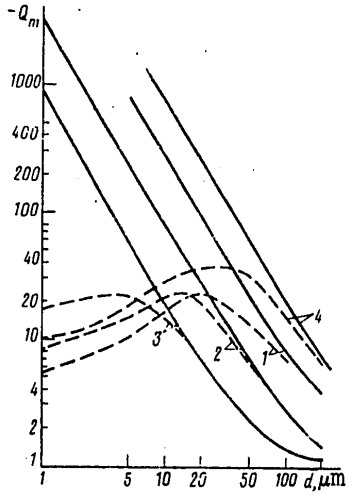

Fig. 5

The frequency dependence Q_{mm} (solid lines) and the dependence on parameters d_m (dot-dash line) and ρ_{mm} (dotted line) for various values of W: 1-W=0.5 μm, 2-W=1 μm, 3-W=5 μm.

in the metal and so increases in proportion to $(W \cdot d)$. In the intervals of values $0.5\ \mu m \leq W \leq 5\ \mu m$ and $1\ \mu m \leq d \leq 100\ \mu m$, corresponding, in general, to the region of low-frequency waves (fig. 2), the values of ρ_m are within the limits of $4 \times 10^{-3} - 10^{-1}\ \Omega \cdot cm$.

In accordance with fig. 4, losses in the semiconductor fall with decreases in d, but the role of losses in the metal increases, which limits the maximum attainable distributed Q-factor with values of $Q_{mm}=20-50$. The latter are attained with a fixed thickness $d=d_m$. The dependence of d_m and Q_{mm} on f and the thickness of the dielectric layer W is shown in fig. 5, where the optimal values of the specific resistance ρ_m corresponding to d_m are also cited. When W is small, the value of Q_{mm} decreases continuously with the frequency. For average W Q_{mm} is slightly dependent upon f, and for large W and f Q_{mm} increases in proportion to f.

In the analysis cited above the current surges that exist in an actual line in proximity to the edge of a strip are not taken into account. A consideration of such an irregular distribution of current in the metallic strip of a MDSM-line leads to serious mathematical complications. However, the exact computation of the losses in a normal microstrip line has shown that when using the relation $b/(W+d)=10$ the rise in the losses due to the uneven distribution of current comprises 25%. With the growth of $b/(W+d)$ this value drops.*

As the results of the current work indicate, it is necessary to take into account the losses in the semiconductor backing as well as the losses in the metallic conductors in order to correctly compute the attenuation of electromagnetic waves in the SHF range in a line of MDSM composition. Consideration of these losses makes it possible to determine the optimal parameters of the structure (specific resistance and the geometric dimensions of the backing) for which the losses are minimal. For an MDSM structure in the frequency range of 3-30 GHz the optimal values of the specific resistance of the semiconductor backing is $(1-6) \cdot 10^{-2}\ \Omega \cdot cm$ with the optimal value for the thickness of the backing being 5-20 μm.

*The growth of the losses in metallic conductors in a microstrip line with $\epsilon=10$ was carried out by A. G. Chursin.

BIBLIOGRAPHY

1. Guckel, H.; Brennan, A. P.; and Paloz, J. IEEE TRANS., MTT-15, No 8, 1967, p 468.

2. Ho, I. T., and Mullick, S. K. IEEE J., SC-2, No 4, 1967, p 201.

3. Hasegawa, H.; Furukawa, M.; and Yanai, H. IEEE TRANS., MTT-19, No 11, 1971, p 869.

4. Hudges, G. B., and White, P. M. "Instruments Based on Nonsymmetric Strip Lines With MDS Structure and Shottky Barrier," TIIER, Vol 60, No 12, 1972, p 127.

5. Guenther, U., and Voges, E. ARCH. ELEKTR. UEBERTRAG., Vol 27, No 3, 1973, p 131.

6. Hambleton, K. G., and Robson, P. N. INT. J. ELECTRONICS, Vol 35, No 2, 1973, p 225.

7. Jages, D.; Rabus, W.; and Eickhoff, W. SOLID STATE ELECTRONICS, Vol 17, No 8, p 777.

8. Egorychev, V. P., and Pavel'ev, D. G. "Semiconductor Devices," ELEKTRONNAYA TEKHNIKA, Ser 2, Vyp 4, No 86, 1974, p 69.

[23-9512]

9512
CSO: 1860

UDC 621.396.049.77

CONSIDERATION OF DESIGN AND TECHNOLOGICAL FEATURES IN THE REALIZATION OF AN ELECTRONICALLY TUNED MATCHED FILTER FOR THE SELECTION OF A COMPLEX SIGNAL

Kiev IZVESTIYA VUZOV RADIOELEKTRONIKA in Russian Vol 22 No 8, 1979 pp 60-64

[Article by N. I. Smirnov and Yu. A. Karavayev]

[Text] The authors examine the technological and design problems involved in developing an electronically tunable matched filter on acoustic surface waves. A complex signal is selected, and the interference immunity is calculated for the matched filter with the selected signal.

Matched filters (MF) on acoustic surface waves are widely used for reception of complex phase-keyed signals with a long base (up to 1000) [Ref. 1, 2, 3, 4]. The matched ASW filter consists of a piezoelectric acoustic line on which interdigital electroacoustic surface wave transducers are integrally sputtered with taps connected to a summing line [Ref. 5]. However, some electronic systems require tuning the MF on ASW from one received signal to another.

For binary phase-keyed signals, the phase is rotated through 180° at the tap by changing the polarity of tap connection to the summing line. This switching of an electronically tunable MF (ETMF) can be realized on p-i-n diodes [Ref. 6]. A block diagram of the ETMF is shown in Fig. 1, where *Вх* is the input, *Вых* is the output, *ОР* is the reference register, *ОС* is the reference signal, *КЭ* are commutating elements, *Вх ВШП* and *Вых ВШП* are the input and output interdigital transducers respectively. The ETMF is controlled by the reference register in which the reference signal is recorded. The ETMF can be made as a large HIC on an acoustic line, using nude p-i-n diodes and a semiconductor IC reference register. One possible diode switch

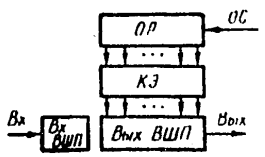

Fig. 1

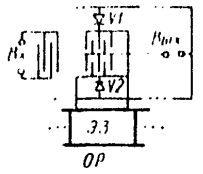

Fig. 2

is shown in Fig. 2, where *Вх* is the input, *Вых* is the output, *ОР* is the reference register and *ЭЗ* is a delay component. One of the p-i-n diodes V1 or V2 is engaged depending on the state of each flip-flop of the reference register. Thus in the working state the number of engaged p-i-n diodes will be equal to the number of taps being switched. The power that controls a single p-i-n diode averages 20-50 mW, and may amount to several watts where there are more than 50 taps to be switched.

A single switch element can be used to switch a number of taps of a delay line (*ЭЗ* in Fig. 2) in a radio system with limited power consumption to reduce the number of commutated components (this simultaneously simplifies the construction of the ETMF as well).

Then the pseudorandom sequence A, which we call the carrier and which is the basis for forming a binary complex phase-keyed signal of duration $N_{ЭН}$, is broken down into $N_{ЭМ}$ segments; $A = \{d_i\}_{i=1}^{N_{ЭН}}$, where the d_i are symbols of the sequence and take on values of +1 or -1. The carrier may be a pseudorandom sequence such as an M-sequence or a re-formed sequence (RFS) [Ref. 1].

The symbols of the carrier that fit into each of the segments are simultaneously keyed by another pseudorandom sequence $B = \{b_j\}_{j=1}^{N_{ЭН}}$, called the modulating sequence, the b_j taking on values of +1 or -1. Thus the resultant sequence will be a sequence of products $d_i b_i$ (Fig. 3), where T_n is signal duration, $T_э$ is the duration of an elementary pulse, T_M is the duration of a segment, i. e. the length of a pulse of the modulating sequence, *НП* is the carrier sequence, *МП* is the modulating sequence, and *РП* is the resultant sequence.

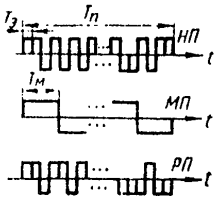

Fig. 3

Considering the possibilities for MF switching, the set of resultant sequences of duration $N_{ЭМ}$ is determined by the set of modulating sequences, and there is no change in the carrier sequence.

Let us analyze the kinds of correlation properties that would be shown by signals formed on the basis of the resultant sequences. For two arbitrary resultant processes $S_l = \{d_i b_j^l\}$ and $S_k = \{d_i b_j^k\}$, where the l and k denote certain modulating sequences out of the possible set, each spike of the correlation function (CF) is formed as a sum of μ products of the type $d_i b_j^l d_{i+p} b_{j+h}^k$. The subscripts p and h denote the number of the relative shift between the sequences (spike number).

For an autocorrelation function (ACF) $l = k$, and for a mutual correlation function (MCF) $l \neq k$. For aperiodic CF the number μ takes on values from 1 to $N_{ЭН}$ for different spike numbers; for periodic, mixed-periodic and meander-inverted CF $\mu = N_{ЭН}$ for all spikes. The mathematical expectation of the modulus of the amplitude of the spikes [Ref. 7, 8] for periodic CF (except for the AFC of M-sequences) in the case of random and pseudo-random sequences is $m(|u_B|) = 0.8\sqrt{N_{ЭН}}$, the standard deviation of the modulus of amplitude of the spikes is $\sigma(|u_B|) = 0.6\sqrt{N_{ЭН}}$, and the standard deviation of the amplitude of the spikes is $\sigma(u_B) = \sqrt{N_{ЭН}}$, while the corresponding quantities for an aperiodic function are $m'(|u_B|) = 0.5\sqrt{N_{ЭН}}$, $\sigma'(|u_B|) = 0.5\sqrt{N_{ЭН}}$, and $\sigma'(u_B) = 0.7\sqrt{N_{ЭН}}$ respectively.

The largest spikes have an amplitude $u_{Bmax} = (3-5)\sqrt{N_{ЭН}}$. A coefficient equal to 3 corresponds to $N_{ЭН} < 200$, and with $N_{ЭН} > 200$ gradually increases to 5 with probability of occurrence of <0.1% [Ref. 8].

In the case of a zero time shift $\tau = 0$ the mutual correlation function has a spike equal to

$$u_0 = \sum_{i=1}^{N_{ЭН}} \sum_{j=1}^{N_{ЭМ}} d_i b_j^l d_{i+p} b_{j+h}^k = \frac{N_{ЭН}}{N_{ЭМ}} \sum_{j=1}^{N_{ЭМ}} b_j^l b_j^k,$$

where $p = 0$, $h = 0$, $d_i d_{i+p} = 1$.

Thus the spike u_0 will be determined by the correlation properties of the modulating processes $\{b_j^l\}$ and $\{b_j^k\}$ that are formed on the basis of pseudorandom or random sequences. The mathematical expectation of the modulus of the amplitude of the spike when their relative time shift is $\tau = 0$ is

$$m(|u_0|) = (N_{ЭН}/N_{ЭМ})\, 0{,}8\sqrt{N_{ЭМ}} = 0{,}8N_{ЭН}/\sqrt{N_{ЭМ}}.$$

In an analogous way we get $\sigma(|u_0|) = 0.6N_{ЭН}/\sqrt{N_{ЭМ}}$, $\sigma(u_0) = N_{ЭН}/\sqrt{N_{ЭМ}}$, and $u_{0Bmax} = (3-5)N_{ЭН}/\sqrt{N_{ЭМ}}$.

By using these expressions, we can estimate the extent to which the correlation properties of resultant sequences change in the absence of a time shift as compared with an arbitrary time shift. For this purpose, Fig. 4 shows plots of the change in standard deviation of spikes $\sigma(u_0)$ as a function of $N_{ЭН}$ for a zero shift (curve 1) and for other shifts (curve 2) normalized with respect to $N_{ЭН}$. The curves for $\sigma(|u_B|)$ and $m(|u_B|)$ as dependent on $N_{ЭН}$ behave like $\sigma(u_B)$ since they differ only by a constant coefficient. An analysis of Fig. 4 shows that the maximum level of mutual interference will occur in the absence of a time shift between the reference and received sequences, i. e. when we have u_0 if the modulating sequence is random or pseudorandom. This can be

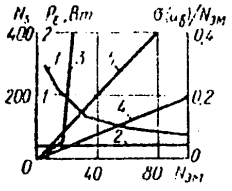

Fig. 4

explained by the circumstance that the spikes of the MCF are defined as for a pseudorandom sequence with $N_{ЭН}$ at all time shifts τ except $\tau = 0$.

An increase in the level of lateral spikes of the MCF at time $\tau = 0$ due to segmental commutation of the MF taps is determined from the expression

$$K = u_{0\text{в max}}/u_{\text{в max}} = (0{,}6 \div 1)\sqrt{N_{\text{эм}}/N_{\text{эм}}},$$

i. e. the greater the number of segments being commutated, the lower will be the loss of interference immunity as compared with the case of commutation of each element of the carrier sequence. Interference immunity can be improved by using modulating processes that are orthogonal at $\tau = 0$ such as Reed-Müller, Stiffler, Welty and Golay sequences [Ref. 1]. Although mutual interference is eliminated in this case, nevertheless the set of signals N_S is reduced, and for each type of modulating sequence $N_S = 2N_{ЭМ}$.

Fig. 4 shows the way that the size of the signal set N_S depends on $N_{ЭМ}$ for pseudorandom signals based on re-formed sequences (RFS) (curve 3) and Reed-Müller (MS) sequences (curve 4). The RFS set is determined from the expression $N_S = N_{ЭМ}N_M^2/2$, where N_M is the number of M-sequences at a given $N_{ЭМ}$. The same figure shows the way that power consumption P_Σ [in watts] in the MF depends on $N_{ЭМ}$ when tap segment commutation is being handled with a controlling power of 25 mW for one switching diode (curve 5).

Let us evaluate to what extent there will be a change in the interference immunity of a data transmission system (DTS) with code separation and with free access of subscribers where there is a change in $N_{ЭМ}$ and the type of modulating sequence as compared with a DTS in which commutation of each individual pulse of the carrier is possible, or the equivalent DTS with resultant sequences in which processes that are orthogonal at $\tau = 0$ are used as modulating sequences. The interference immunity of the DTS is determined by the probability of error at the output of the threshold device to which a mixture of signal and interference is sent from the MF output:

$$p_{\text{ош}} = 1 - \Phi(1/\sqrt{q_{\text{вых сф}}}),$$

where $\Phi(x) = \frac{2}{\sqrt{\pi}}\int_0^x \exp(-t^2)\,dt$ is the error integral, $q_{\text{ВЫХ СФ}}$ is the ratio $P_C/P_{\Sigma\text{П}}$ at the ETMF output, P_C is signal power, $P_{\Sigma\text{П}}$ is the total power of interference at the MF output [Ref. 9]

$$\sigma^2_{\Sigma\text{п}} = \sigma^2_{\text{фл}} + u^2_{\text{в max}} + N_{\text{адр}}\sigma^2(u_{\text{в}}),$$

since it is determined by the sum of the variances of independent random processes: fluctuation noise $\sigma^2_{\text{ФП}}$, the power of the maximum lateral spikes $u^2_{\text{Вmax}}$ and the variance of the lateral spikes of the MCF from $N_{\text{адр}}$ simultaneously operating stations $N_{\text{адр}}\sigma^2(u_{\text{В}})$.

For the resultant sequences we have (version 1):

$$q_{\text{вых сф1}} = \frac{N_{\text{эн}}^2}{\sigma_{\text{фл}}^2 + \left(3\frac{N_{\text{эн}}}{\sqrt{N_{\text{эм}}}}\right)^2 + N_{\text{адр}}(\sqrt{N_{\text{эн}}})^2},$$

where it is taken into consideration that the maximum spike of the MCF is equal to $u_{B\max} = 3N_{\text{ЭН}}/\sqrt{N_{\text{ЭМ}}}$, $\sigma(u_B) = \sqrt{N_{\text{ЭН}}}$, and the powers of the interfering signals from operating stations are each equal to the power of the received signal. The maximum MCF spike is determined by the correlation properties of the modulating sequence, which have short duration ($N_{\text{ЭМ}} < 200$), and therefore a coefficient of 3 is taken. For the case of a DTS with signals in which each symbol of the carrier sequence could be commutated, the maximum spike will be equal to $5\sqrt{N_{\text{ЭН}}}$, since $N_{\text{ЭН}}$ is a quantity measured in hundreds or thousands, and hence we have (version 2):

$$q_{\text{вых сф2}} = \frac{N_{\text{эн}}^2}{\sigma_{\text{фл}}^2 + (5\sqrt{N_{\text{эн}}})^2 + N_{\text{адр}}(\sqrt{N_{\text{эн}}})^2}.$$

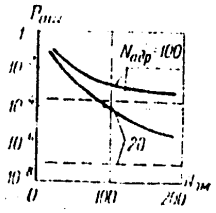

Fig. 5

Fig. 5 shows plots of $p_{\text{ош}}(N_{\text{ЭМ}})$ for version 1 (solid line) and version 2 (broken line) and various $N_{\text{адр}}$. It was assumed that fluctuating noises exceed signal power by a factor of 20. It can be seen from the curves that with increasing $N_{\text{ЭМ}}$ and $N_{\text{адр}}$ there is a reduction in difference between the first and second versions of the DTS with respect to noise immunity, although the version of the DTS with a resultant sequence remains poorer.

We note in conclusion that segment commutation of taps can reduce the required number of switching diodes by a considerable factor, and in this way can appreciably simplify the design of the large HIC, and also reduce the power consumption for commutation by a considerable factor. However, commutation of the tap segments of an interdigital transducer in accordance with the law of a binary keying sequence means that the signal set is determined by the set of the keying process, which is several times smaller than that of the carrier sequence. Besides, this type of commutation is detrimental to the autocorrelation and mutual correlation properties of the signals.

REFERENCES

1. V. B. Pestryakov, ed., "Primeneniye shumopodobnykh signalov v sistemakh peredachi informatsii" [Use of Noise-Like Signals in Data Transmission Systems], Moscow, "Sovetskoye radio", 1973.

2. L. Ye. Varakin, "Teoriya sistem signalov" [Theory of Signal Systems], Moscow, "Sovetskoye radio", 1978.

3. S. S. Karinskiy, "Ustroystva obrabotki signalov na ul'trazvukovykh poverkhnostnykh volnakh" [Devices for Signal Processing on Ultrasonic Surface Waves], Moscow "Sovetskoye radio", 1975.

4. S. L. Zabuzov, T. S. Ivshina, G. F. Sirotin, "Formation and Compression of Complex Signals with Product of Duration Times Spectrum Width Equal to 1000," IZVESTIYA VUZOV RADIOELEKTRONIKA, Vol 19, No 4, 1976, p 125.

5. N. I. Smirnov, V. I. Gvozdev, N. N. Zalichev, "Reliability of Optimum Processing Devices Based on Quartz Surface-Wave Delay Lines," RADIOELEKTRONIKA, No 8, 1975, p 117.

6. M. Ye. Il'chenko, V. G. Osipov, "Electrically Controlled Microwave Switches Based on Semiconductor Diodes," IZVESTIYA VUZOV RADIOELEKTRONIKA, Vol 20, No 2, 1977, p 5.

7. V. S. Gutin, "Correlation Properties of Random Binary Sequences," RADIOTEKHNIKA I ELEKTRONIKA, Vol 18, No 2, 1973, p 409.

8. N. I. Smirnov, "Characteristics of Two-Dimensional Correlation Functions of Complex Signals," RADIOTEKHNIKA, Vol 29, No 12, 1974, p 20.

9. N. I. Smirnov, "Interference Immunity of Electronic Systems with Complex Signals in the Pulse and cw Modes," IZVESTIYA VUZOV RADIOELEKTRONIKA, Vol 20, No 11, 1977, p 125.

[8144/0670-6610]

6610
CSO: 8144/0670

FIFTH INTERNATIONAL SYMPOSIUM ON ELECTROMAGNETIC COMPATIBILITY ANNOUNCED

Moscow ELEKTROSVYAZ' in Russian No 10, 1979 p 61

[Article: "Fifth International Symposium on Electromagnetic Compatibility"]

[Text] From 17 through 19 Sep 80 in the city of Wroclaw (Polish People's Republic) will be held the next international symposium on electromagnetic compatibility (EMS). The topics of papers are as follows: prediction of the influence of noise in equipment and systems; electromagnetic fields, antennas and the propagation of radio waves; EMS in wire communications; control of a spectrum by using computers; noise rejection and sensitivity; economy of the spectrum and influence of new equipment on EMS; lightning and EMS; monitoring the spectrum and direction finding by utilizing computers; cooperation in the area of EMS on the national and international scales--recommendations, norms and standards; biological influence of high-frequency energy; shielding and filters; mathematical modeling in research on EMS; methods and equipment for measuring; electromagnetic contamination and individual noise sources; and planning radio systems.

While the symposium is being held an exhibition is being organized, at which the following will be demonstrated: modern measuring equipment; noise suppression elements for domestic, industrial and transportation equipment; shielded compartments; shielding and absorbing materials; modern equipment for monitoring occupation of the spectrum; non-emitting and noise-immune equipment; methods of planning EMS and monitoring noise; as well as literature on EMS.

The official languages of the symposium are English and Russian.

[62-8831]

8831
CSO: 1860

UDC 621.314.6

DISCRETELY CONTROLLED FERROMAGNETIC ELEMENTS FOR THE CONVERSION OF ELECTRIC POWER PARAMETERS

Moscow DISKRETNO-UPRAVLYAYEMYYE FERROMAGNITNYYE ELEMENTY DLYA PREOBRAZOVANIYA PARAMETROV ELEKTROENERGII in Russian 1979 signed to press 11 May 79 pp 2, 191-192

[Annotation and table of contents from book by Valentin Petrovich Obrusnik, Izdatel'stvo Nauka, 1100 copies, 192 pages]

[Text] ANNOTATION

The subject of this monograph is the theory and planning of converters in automatic control systems. The author discusses the following subjects: the physical principles of ferromagnetic elements, the theory of the processes and the characteristics of pulse-switched ferromagnetic elements with pulse magnetization, research principles, and energy indicators. He also presents and discusses examples of control circuits based on discretely controlled elements.

This book is intended for specialists in instrument building and automatic control. Figures 68; references 133.

TABLE OF CONTENTS

	Page
Introduction.	3
Chapter 1. Physical Principles of Discretely Controlled Ferromagnetic Elements	8
1.1. Physical Nature and Theoretical Principles of Discrete Methods of Controlling Ferromagnetic Elements	10
1.2. Basic Properties and Principles of the Construction of Pulse-Magnetized Ferromagnetic Elements.	17
1.3. Basic Properties and Principles of the Construction of Pulse-Switched Ferromagnetic Elements.	23
1.4. Ferromagnetic Elements With Discretely Controlled Feedback	28
1.5. Classification and Comparative Evaluation of Discretely Controlled Ferromagnetic Elements	32

Page

1.6. Basic Problems in the Area of Research and Development Work on Discretely Controlled Ferromagnetic Elements 37

Chapter 2. Theory of the Processes and the Basic Characteristics of Pulse-Switched Ferromagnetic Elements. 40
2.1. Single-Switch Artificially Switched Magnetic Valve Devices Working Under an Active Load 40
2.2. Single-Phase Double-Switch Magnetic Valve Devices With Artificial Switching. 49
2.3. Magnetic-Valve Frequency Doublers. 57
2.4. Output Filters for Magnetic Valve Devices With Artificial Switching. 60
2.5. Three-Phase Voltage Regulators Based on Magnetic Valve Devices With Artificial Switching. 63
2.6. Special Features of the Dynamic Modes of Magnetic Valve Devices With Artificial Switching. 63

Chapter 3. Theoretical Principles of the Investigation of the Electromagnetic Processes in Devices With Pulse-Magnetized Ferromagnetic Elements. 67
3.1. Basic Propositions of the Stage-by-Stage Method of Investigating Devices With Pulse-Magnetized Ferromagnetic Elements 68
3.2. Methodology for Investigating Processes and Characteristics in Control Circuits 71
3.3. Theory of Stationary Processes of Control Circuits 79
3.4. Methodology for Investigating Processes and Characteristics in Power Circuits 86
3.5. Constructing Equivalent Circuits for the Power Circuits of Pulse-Magnetized Ferromagnetic Elements. 95

Chapter 4. Analysis of the Electromagnetic Processes, Basic Characteristics and Power Indicators of Pulse-Magnetized Ferromagnetic Elements. 99
4.1. Methodology for Investigating Quasi-Steady-State Processes and Their Indicators in Connection With Numerical Analysis on a Digital Computer 99
4.2. Analysis of Integral Characteristics 107
4.3. Criteria and Indicators of Harmonic Analysis 110
4.4. Characteristics of the Current Modulation Factor of a Magnetizing Circuit. 113
4.5. Power Indicators and Their Characteristics 115
4.6. Analysis of the Dynamic Modes of Pulse-Magnetized Ferromagnetic Elements 121
4.7. A Brief Discussion of the Nonsymmetrical Models of Pulse-Magnetized Ferromagnetic Elements. 130

Chapter 5. Structure and Planning Elements of Discretely Controlled Ferromagnetic Elements 133

Page

5.1. General Structure of the Construction of Discretely Controlled Ferromagnetic Elements and Its Basic Elements 133
5.2. Construction of the Control Circuits of Pulse-Magnetized Ferromagnetic Elements 135
5.3. Construction of Pulse-Switched Ferromagnetic Elements 143
5.4. High-Speed Feedback for Discretely Controlled Ferromagnetic Elements 149
5.5. Calculating Switching Devices for Discretely Controlled Ferromagnetic Elements 151
5.6. Calculating the Basic Parameters of the Ferromagnetic Frequency of Discretely Controlled Ferromagnetic Elements 156

Chapter 6. Examples of Control Systems Based on Discretely Controlled Ferromagnetic Elements 166
6.1. Single-Phase Voltage Stabilizers 167
6.2. Three-Phase Voltage and Current Regulators 170
6.3. Voltage Converters Based on Magnetic Valve Devices 176
6.4. Comparative Indicators and Prospects for the Use of Discretely Controlled Ferromagnetic Elements in Systems for Controlling and Converting Electric Power Parameters 178

Bibliography 185

11746
CSO: 1860

UDC 621.373.52:534

OSCILLATION SOURCES BASED ON SURFACE ACOUSTIC WAVES

Moscow RADIOTEKHNIKA in Russian No 10, 1979 pp 40-43 manuscript received 18 Jun 79

[Article by A.V. Ryzhkov]

[Text] Acoustoelectronics has been gaining more and more importance in solving the problem of microminiaturizing radioelectronic equipment, especially frequency selective devices. By employing devices which utilize surface acoustic waves (PAV's) it has been possible to form a network of frequencies directly in the range from dozens of MHz to 1.5 to 2 GHz. Most widespread are single-frequency (fig 1a) and multifrequency (fig 1b) oscillators, the stability of whose frequency is determined by the stability of a PAV delay line (LZ) included in the feedback circuit of a broadband amplifier [1]. Instead of an LZ it is possible to include also precision resonators, filters or combs of filters. It is known [2] that in certain crystalline materials serving as a substrate for PAV devices right up to the microwave band it is possible to obtain a Q on the order of 10^4 and more. Therefore the positive aspects of PAV oscillators are obvious, since they are determined chiefly by the selective elements.

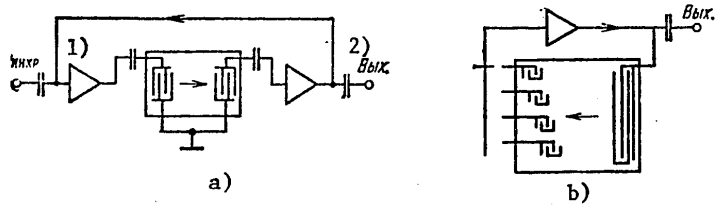

Figure 1.

[Key on following page]

Key:
1. Sync
2. Output

In [2] it is reported that longterm stability (ageing) has been observed close to 10^{-6} per month, which is comparable with the stability of relatively high-Q solid quartz resonators (KR's), and approximately an order of magnitude below the stability of precision KR's. As studies have demonstrated, the temperature coefficient of frequency (TKCh) of PAV oscillators with an LZ utilizing an ST-cut quartz substrate equals (1 to 2)$\cdot 10^{-5}$, which is approximately 1.5 to two orders of magnitude worse than the TKCh of precision quartz oscillators (KG's). For the purpose of reducing sensitivity to changes in temperature, LZ's are designed with a substrate made of a material causing the propagation of PAV energy in two directions, for which the temperature coefficients of the delay have opposite signs.

Let us compare PAV oscillators with KG's with regard to shortterm frequency stability. The spectral power density of phase fluctuations of an oscillator with a filter in a feedback circuit can be represented in the form

$$S_{\varphi}[F] = \frac{NkT}{P_c}\left[F_{\alpha}F_f^2F^{-3} + F_f^2F^{-2} + F_{\alpha}F^{-1} + 1\right],$$

where N is the transistor's noise factor, k is the Boltzmann constant, T is the absolute temperature, P_s is the power in the amplifier's input, F_{α} is the modulation frequency at which the flicker noise level is equal to the level of the white noise, F is the modulating frequency and $F_f = f_0/2Q$ is the transmission band of the feedback circuit.

In fig 2 are given graphs of calculated (solid lines) and experimental (dotted lines) dependences of $S_{\phi}[F]$ for:

A PAV oscillator with f_0 = 490 MHz, a PAV route length of 300 λ, conversion losses of 20 dB, N = 6 dB, and P_s = 50 μW--curve 1 [2].

A KG with f_0 = 100 MHz, P_s = 100 μW, N = 3 dB--curves 2.

A KG with f_0 = 5 MHz, P_s = 10 μW, N = 3 dB--curves 3.

A system consisting of a KG with f_0 = 5 MHz and an ideal 100-fold frequency multiplier--curve 4 [3].

In PAV oscillators is possible optimization (reduction) of the noise level by more than 10 dB as a result of reducing losses in the LZ (which equal more than 20 dB). It is possible to achieve some reduction in losses in the LZ by, for example, dividing the output transducer into at least two transducers placed at equal distances on both sides of the input transducer. In spite of the possible reduction of losses, PAV oscillators, as compared with precision KG's and a series chain of multipliers, especially

in the close-range zone, do not have advantages with respect to spectral purity. However, the existence of PAV structures makes it possible to create highly practical miniature oscillating devices with characteristics approximating the characteristics of KG's. It must be mentioned that with an increase in frequency the electrical characteristics of KR's deteriorate drastically, especially aging and activity, and the creation of KG's for the microwave band as a complex problem, since difficulties arise both in the excitation of harmonic KR's and in the creation of KR's for a strictly determined frequency. The transmission bands of KR's are very short and therefore the synchronization bands of KG's are also short, and the long-term frequency stability of free oscillators in a number of instances is insufficient.

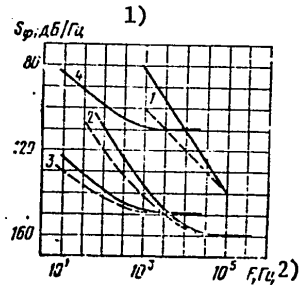

Figure 2.

Key:
1. dB/Hz
2. Hz

The possibility of synchronizing a PAV oscillator has been investigated by using the example of an oscillator with f_0 = 69.417 MHz (fig 1a) and a transmission band for the LZ in terms of the 3 dB level of approximately 4 MHz. The region of synchronization is shown in fig 3. The capture band can be determined here from the familiar equation for an oscillator with a filter circuit in the feedback circuit [4]:

$$2\Delta f = f_0 U_{синхр} Q U_г \cos\varphi,$$

where U_{sinkhr} is the synchronizing voltage, U_g is the voltage of the oscillator in the free mode, Q is the quality factor of an equivalent band filter, and ϕ is the phase shift in the feedback circuit.

The asymmetry of the synchronization band in relation to f_0 is explained by the existence of a delay in oscillation in the feedback loop and by the asymmetry of the LZ's amplitude-frequency characteristic (AChKh). The broader the transmission band of the LZ, the broader also the region of synchronization; however, with an increase in the transmission band losses

in the LZ also grow. It is advisable to use oscillators with a broadband LZ in the feedback loop only in the synchronization mode, since in the free mode, when the power supply is turned on, they can be excited at any mode for which the phase advance equals $2\pi L$. This property is utilized in multifrequency oscillators (fig 1b), where by means of a control it is possible to shift from one frequency to another, whereby the stability of the frequency remains almost the same as in a single-mode oscillator with a fixed frequency, and the amplitude of the fundamental maximum, even without external selective devices, exceeds the parasitic components by 60 dB and more. Synchronization is accomplished similarly to synchronization in single-frequency oscillators with the only difference that in this case the synchronizing effect has a linear spectrum similar to the frequency spectrum of the waves generated. The level of secondary components in the output oscillation, depending on the point of application of the synchronizing effect, can be low, since the output transducers, in turn, can be additional selective filters.

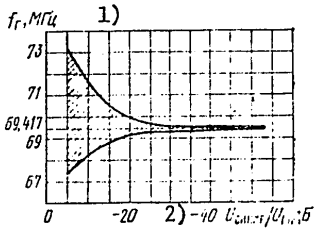

Figure 3.

Key:
1. f_g , MHz
2. U_{sinkhr}/U_g , dB

The utilization of synchronized PAV oscillators has been conducive also to the development of frequency synthesizers, especially designed by the method of direct synthesis. The key element in these is a comb filter, generally containing K pairs of opposing-pin transducers fabricated so that K orthogonal filters are formed. The transmission frequency of one channel matches the infinite attenuation (nulls) of all the other channels. The theoretical AChKh of a typical filter channel has the form

$$\frac{\sin x}{x}\,\frac{\sin 2x}{2x}, \qquad (1)$$

where $x = \pi(f - f_0)/f_s$, f is the frequency in the input, f_0 is the transmission frequency of the filter, and f_s is the network spacing, equal to the frequency of the reference KG.

The first factor in (1) is determined by the input (short) transducer, and the second by the output (long) transducer. When both transducers have maximum attenuation for the transmission band, the losses introduced are almost 60 dB lower than the level of losses at the transmission frequency.

For the purpose of synthesizing the required frequencies, directly to the block of PAV filters is fed a uniform spectrum of comb shape, formed from oscillation of the reference KG at a frequency of $\Omega = 2\pi f_s$. The frequency spectrum, for example, of a train of pulses of subnanosecond length (τ) with amplitude E, the repetition rate, T, of which equals the interval between nulls of the PAV filter, is determined from the equation

$$e(t) = E\left[\frac{\tau}{T} + \frac{2}{\pi}\sum_{n=1}^{\infty}\frac{\sin\frac{\pi\Omega\tau}{2}}{n}\cos(n\Omega t - \varphi_n)\right], \tag{2}$$

where the amplitude of the voltage of the n-th harmonic component equals

$$U_n = \frac{2E}{n\pi}\left|\sin\frac{n\Omega\tau}{2}\right|; \tag{3}$$

$$\varphi_n = \operatorname{arctg}(1-\cos n\Omega\tau)/\sin n\Omega\tau = n\Omega\tau/2 \tag{4}$$

is its phase.

In [2] is described a quite compact frequency synthesizer designed on the basis of a block of 16 PAV filters (measuring 2.5 X 0.9 cm) and a miniature high-frequency switching matrix consisting of p-i-n diodes, executed according to the "silicon on sapphire" technology, measuring 2.5 X 0.25 cm. This synthesizer, employing substrates with a YZ cut of $LiTaO_3$ has a spectral purity characterized by a level of secondary regular components relative to the fundamental oscillation of -55 dB in the frequency band of 520 to 650 MHz, and by a network spacing of 0.5 MHz. The introduced losses for each interconnected PAV filter (without taking into account the switching matrix) nominally equal 25 dB. The level of the input oscillation for each filter is determined from (3).

It is possible to improve filtration characteristics by combining PAV filters of resonators electrically or acoustically. Cascade connection of filters is effective only when the fundamental frequencies differ by a small fraction of the transmission band of an individual filter. Slightly pronounced inhomogeneities of the substrate or variations in technology

can be the cause of variance with respect to the mid-band frequency; therefore after fabrication it is necessary in one way or another to carry out quite precise tuning. Here it is necessary to take into account such factors as ageing and the temperature range. The most effective solution for improving the spectral characteristics of the output oscillation of a synthesizer is a cascade connection with filters of synchronized PAV oscillators [5], because of which it is possible to filter harmonics of the reference oscillator by 80 to 90 dB (cf. fig 3) and to achieve a low white noise level in the structure of output oscillations. Filters with such parameters do not yet exist in the VHF and UHF wavebands.

Bibliography

1. Rechitskiy, V.I. and Singur, Ye.K. ZARUBEZHNAYA ELEKTRONIKA, No 3, 1978.

2. TIIER, Vol 64, No 5, 1976.

3. Ryzhkov, A.V. and Kremnev, Yu.V. RADIOTEKHNIKA, Vol 31, No 12, 1976.

4. Samoylo, K.A. "Sinkhronizatsiya generatorov garmonicheskikh kolebaniy i parametricheskiye generatory i usiliteli" [Synchronization of Generators of Harmonic Oscillations and Parametric Oscillators and Amplifiers], Moscow, 1967.

5. Ryzhkov, A.V., Slastunov, Ye.A. and Yerokhin, M.V. Patent No 634447 with priority from 16 May 1977.

[59-8831]

8831

CSO: 1860

UDC 621.396

SOME ASPECTS OF THE DESIGN OF CLOSE-RANGE NOISE SIGNAL RADAR SETS WITH INTEGRATED COVERAGE

Moscow RADIOTEKHNIKA in Russian No 10, 1979 pp 31-33 manuscript received 9 Mar 79

[Article by V.V. Grigorin-Ryabov, V.I. Shelukhin and O.I. Shelukhin]

[Text] The design of close-range radar sets (RLS's) intended for detecting stationary objects located within the limits of a fixed region has a number of specific features. Let us discuss the design principle of this equipment, operating with noise-type echo signals. These RLS's consist of a spatially separated receiver and transmitter placed at the focal point of an ellipse whose generatrix passes through the geometrical center of the territory monitored (fig 1). Correlation processing is assumed in the equipment, so that for the signal in the input of the actuating equipment (threshold element) it is possible to write

$$B(\tau)_{\text{вх. пу}} = K\int_0^T S_c(t-\tau_{\text{задер1}})\,S_{\text{оп}}(t-\tau_{\text{задер2}})\,dt,$$

where

$$\tau_{\text{задер}_1} = \frac{1}{c}(R_1+R_2) = \frac{1}{c}\left(\sqrt{(a+x)^2+(b+y)^2+h^2}+\sqrt{(a-x)^2+(b+y)^2+h^2}\right).$$

[PU = threshold element, vkh = input and zader = delay.]

When the object is located on the generatrix of the ellipse, for any of its positions the following equation is valid

$$\tau_{\text{задер}} = \frac{1}{c}(R_1+R_2) = \text{const}.$$

Thus, this kind of processing of the reflected signal does not make possible resolution with regard to the angular coordinate. However, utilizing the directional properties of the transmitting, $F_{per}(\theta)$, and receiving, $F_{pr}(0)$, antennas, it is possible to reduce the resolution range to the dimensions of the region monitored. Resolution in terms of range is made possible by selection of the echo signal, since the directional properties of antennas in this case are but slightly pronounced. The continuous operating mode is discussed for a close-range noise signal RLS. It is obvious that the shorter the lengthwise dimensions of the region monitored, the more broadband must be the echo signal. Since in the equipment is assumed correlation processing of the signal with a threshold actuator, it is necessary to employ as the echo signal signals whose autocorrelation function will be as close as possible to rectangular. Satisfying these properties to the greatest extent, taking into account the simplicity of implementing shaping of the echo signal, are limited-band white noise with a band of $\Delta\omega = \omega_2 - \omega_1$, a spectral density of N_0 and a correlation function of $B(\tau) = \Delta\omega N_0(\sin \Delta\omega\tau/\Delta\omega\tau)$, and signals the autocorrelation function of whose envelope has the form

$$B(\tau) = \exp\left\{-\frac{4}{c^2}\tau^2\right\}. \qquad (1)$$

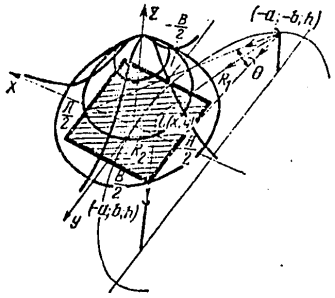

Figure 1.

The most important magnitude characterizing the operation of RLS's of this type is the signal-to-noise ratio, $q = P_s/P_f$, where P_f is the power reradiated by the underlying surface and local objects.

Let us determine the averaged power of the signal reflected from an obstacle, taking into account the indeterminacy of its position within the limits of the fixed region, from the equation

$$P_c = \frac{K_{м.л} K_{м.к} A_0}{XY} \int_0^X \int_0^Y B[\tau(x:y)] F_{пер}^2[\theta(x:y)] F_{пр}^2[\theta(x:y)] \sigma_{пр}\, dx dy, \tag{2}$$

where X and Y are the geometrical dimensions of the detected object; $K_{м.л}$ is the transmission coefficient for the power of the linear section of the receiver; $K_{м.к}$ is the parameter of the correlator; $A_0 = P_\Sigma \lambda^2 D_{пер} D_{пр} / 64\pi^3 R_1^2 R_2^2$; $D_{пер}$ and $D_{пр}$ are the coefficients of the directional effect of the transmitting and receiving antennas, respectively; P_Σ is the radiative power; and $\sigma_{пр}$ is the EOP [?end output] of the obstacle. Similarly for the power of the noise it is possible to write [1]

$$P_\Phi = K_{м.л} K_{м.к} A_0 \int_{-\infty}^{\infty} \int B[\tau(x:y)] F_{пер}^2[\theta(x:y)] F_{пр}^2[\theta(x:y)] V(x:y)\, dx dy, \tag{3}$$

where V(x:y) is the coefficient of reflection from the underlying surface.

In the geometrical interpretation the problem of maximizing q is analogous to maximizing the space concentrated above the region monitored and computed from equations (2) and (3). As is obvious from fig 1, this problem can be reduced to the optimal location of the transmitting and receiving points with fixed characteristics of the echo signal. Thus, in the case presented in fig 1, the integrand is computed for $B[\tau(x:y)]$, having the form of (1), where

$$\tau(x:y) = \frac{\Delta R}{c} = \frac{1}{c}\{\sqrt{(a+x)^2 + (b+y)^2 + h^2} + \sqrt{(a-x)^2 + (b+y)^2 + h^2} - 2\sqrt{a^2 + b^2 + h^2}\},$$

and the equation for the directivity diagram is

$$F_{пр}[\theta(x:y)] = F_{пер}[\theta(x:y)],$$

$$F[\theta(x:y)] = \frac{\sin\left[\frac{1}{2} km \cos[\theta(x:y)]\right]}{\frac{1}{2} km \cos[\theta(x:y)]} (1 + \sin[\theta(x:y)]),$$

$$\sin[\theta(x:y)] = \frac{a(a+x) + b(b+y) - h(z-h)}{\sqrt{(a^2 + b^2 + h^2)[(a+x) + (y+b) + (h+z)]}}.$$

Here $a/b = 2$. The dependence of $q/q_{max} = f(a/b)$ for the signal characteristics indicated and the type of antennas selected is shown in fig 2.

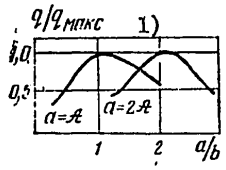

Figure 2.

Key:
1. q/q_{max}

The geometrical interpretation given of the maximization of q makes it possible in each specific instance to optimize the placement of receiving and transmitting antennas in relation to the territory monitored.

Let us consider some questions relating to the implementation of this equipment, viz., the formation of the echo and reference signals, the influence of the spatial separation of the transmitter (receiver) on its efficiency, and an analysis of the filtered signal.

A structural diagram of the RLS [3] is shown in fig 3. The key difficulties involved in shaping an echo signal in the form of a microwave oscillation amplitude modulated by the initial noise are due to nonlinearity of the modulation characteristics of the transmitting channel and the detection errors caused by them, since in the receiver a computation is made of the correlation function between the microwave signal detected and the initial modulating noise delayed for a period τ_0.

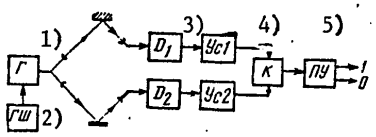

Figure 3.

[Key on following page]

Key:
1. Oscillator
2. Noise generator
3. Amplifier 1
4. Correlator
5. Threshold element

A computation of the correlation function of an echo signal modulated in terms of amplitude and phase by a random process with arbitrary nonlinearity of modulation characteristics is given in detail in [2].

The analysis of the envelopes of correlation functions for particular cases of modulation characteristics, given in [2], demonstrates that the influence of nonlinearity is reflected in narrowing of the correlation functions of the envelope of the echo signal. These causes result in errors in measuring the position of obstacles, which in certain cases is especially dangerous at boundaries of the monitored area. In addition, the instability of the characteristics of delay lines accomplishing delay of the broadband reference noise for a period of τ_0 and lack of agreement of their amplitude-frequency characteristics with the characteristics of the signal result in additional errors with this design.

Free of these disadvantages is an arrangement employing a mirror reflector for the purpose of forming the reference signal. Here, on the ellipse's generatrix at an arbitrary point is installed a mirror reflector, so that the delay of the signal reflected back by it satisfies condition (1). With this method of shaping the reference signal it is possible practically completely to eliminate the influence of the nonlinearity of modulation characteristics on detection characteristics.

Let us dwell in somewhat greater detail on an analysis of the influence of the signal filtered from the transmission channel into the reception channel on the efficiency of the RLS. Let the autocorrelation function of the initial noise equal $B_\xi(\tau)$. Then, assuming that only amplitude modulation of the SHF oscillator is carried out and that the modulation characteristic is linear, after not too complicated transforms we determine the correlation function of the signal in the input of the threshold element, $B_{vkh\ pU}(\tau) = a_1 + a_2 B_\xi(\tau) + a_3 B_\xi(\tau)$, where a_1, a_2 and a_3 are certain coefficients.

Thus, the influence of the filtered signal boils down to broadening of the correlation function, which results in errors in detection at the boundary of the fixed area, which, however, in view of the fact that τ_{pr} = const can be minimized (τ_{pr} is the delay time of the filtered signal).

The equations obtained make it possible to determine the most intelligent coordinates for placement of the antennas of the transceiver of the RLS's discussed.

Bibliography

1. Shelukhin, O.I. IZVESTIYA VUZOV SSSR, SERIYA RADIOELEKTRONIKA, Vol 20, No 5, 1977.

2. Shelukhin, O.I. IZVESTIYA VUZOV SSSR, SERIYA RADIOELEKTRONIKA, Vol 19, No 7, 1976.

3. Grigorin-Ryabov, V.V., Shelukhin, V.I. and Shelukhin, O.I. Patent No 510402.

8831
CSO: 1860

UDC 621.396.677:621.396.96

SOME FEATURES OF THE DEPOLARIZING PROPERTIES OF RADAR TARGETS

Moscow RADIOTEKHNIKA in Russian No 10, 1979 pp 72-74 manuscript received 24 May 79

[Article by L.A. Zhivotovskiy]

[Text] It is known that radar signals are depolarized when reflected from a fluctuating target [1,2]. The depolarization properties of the radar target (RLTs) can be characterized by a "polarization portrait" of the target employing a Poincaré sphere [3]. On the basis of this representation, let us discuss the following problem: With what set of radar system (RLS) radiation polarizations, {h} , will signals reflected from the RLTs be chaotically polarized, i.e., the degree of polarization of reflected signals will equal p = 0 ?

According to [3] with any RLTs with a random symmetric scattering matrix, T , by employing a Poincaré sphere it is possible to compare a certain spherical tetragon, e.g., $A_1A_2A_3A_4$ in fig 1. Here the field of reflected signals can be represented formally as the sum of the fields of four uncorrelated polarized waves and an unpolarized wave:

$$s(t) = \sum_{j=1}^{4} s_{nj}(t) + s_0(t).$$

The intensities of these waves, $s_{pj}(t)$, where $j = \overline{1,4}$, equal, respectively:

$$\left.\begin{aligned} &J_{n1(2)} = |h_{1(2)}|^2\lambda_{1(2)},\ J_{n3(4)} = |h_1h_2\cos\alpha(\sin\alpha)|\lambda_{3(4)},\\ &\lambda_{1(2)} = \left\{\left[\langle|t_{12}|^2\rangle - \langle|t_{11(22)}|^2\rangle\right]^2 + 4\left|\langle t_{12}t^*_{11(22)}\rangle\right|^2\right\}^{\frac{1}{2}},\\ &\lambda_{3(4)} = 2\left[\mathrm{Re}^2(\mathrm{Im}^2)\left(\langle t^*_{11}t_{12}\rangle - \langle t^*_{12}t_{22}\rangle\right) + \left|\langle|t_{12}|^2\rangle + (-)\langle t_{11}t^*_{22}\rangle\right|^2\right], \end{aligned}\right\} \quad (1)$$

where

t_{rn} (r,n = 1,2) are elements of matrix T ; h_1 and h_2 are orthogonal components of vector h on a predetermined polarization base, $|e_1,e_2|$; $\alpha = \arg(h_1/h_2)$; and the angle brackets indicate averaging in terms of time; and the asterisk indicates complex conjugation.

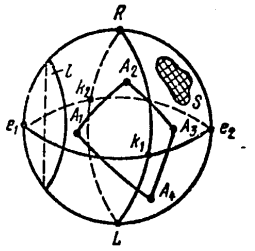

Figure 1.

Polarizations of waves, $s_{pj}(t)$, corrspond to points A_j , whereby points A_3 and A_1 become diametrically opposite with $\cos\alpha < 0$ and $\sin\alpha < 0$, respectively. The positions of points A_j on the sphere are determined by the equations in [3]:

$$\left.\begin{aligned} &A_j = \left\| \begin{matrix} a_{j1} \\ a_{j2} \end{matrix} \right\|, \quad j = \overline{1,4}, \\ &\frac{a_{12(22)}}{a_{11(21)}} = \frac{\lambda_{1(2)} + \langle |t_{12(22)}|^2 \rangle - \langle |t_{11(12)}|^2 \rangle}{2\langle t_{11(12)} t^*_{12(22)} \rangle}, \\ &\frac{a_{32(42)}}{a_{31(41)}} = \frac{\lambda_{3(4)} + 2\,\mathrm{Re}\,(\mathrm{Im})\left(\langle t^*_{12} t_{22} \rangle - \langle t^*_{11} t_{12} \rangle\right)}{2\,(j)\left(\langle \widetilde{t}^*_{11} t_{22} \rangle + (-)\langle |t_{12}|^2 \rangle\right)}. \end{aligned}\right\} \qquad (2)$$

where a_{j1} and a_{j2} are coordinates of A_j on base $|e_1,e_2|$.

Since the polarized component of the field of reflected signals originates as the result of interference of waves, $s_{pj}(t)$ [4], then from (1) it follows that:

An RLTs does not exist for which $p = 0$ with all possible values of h , since for this it is necessary to fulfill the equality $\langle |t_{11}|^2 \rangle = \langle |t_{12}|^2 \rangle = \langle |t_{22}|^2 \rangle = 0$, which is equivalent to the absence of an RLTs.

Let us demonstrate the validity of this statement;

An RLTs does not exist for which $p = 0$ with a set of values of h to which on a Poincaré sphere corresponds a region with an area different from zero, e.g., a certain region S in fig 1.

1. Let us assume that all λ_i except one (λ_r, $r = \overline{1,4}$) equal zero. Then the intensity of the polarized component of the wave, $s(t)$, is $J_p = J_{pr}$ and $J_p = 0$ in the following cases:

a) $|h_1|(|h_2|) = 0$ with $r = 1(2)$.

b) $\cos\alpha$ ($\sin\alpha$) $= 0$ with $r = 3(4)$.

Corresponding to case a) are points e_1 and e_2, and to case b) circles e_1Re_2L and $e_1k_1e_2k_2$ in fig 1.

2. Let us assume that two λ_i differ from zero (λ_r, $\lambda_m \neq 0$, $r,m = \overline{1,4}$). Here it is obvious that $p = 0$ if the polarizations of waves $s_{pr}(t)$ and $s_{pm}(t)$ are mutually orthogonal and $J_{pr} = J_{pm}$, or (with non-orthogonality of these polarizations) with $J_{pr} = J_{pm} = 0$. An analysis of (1) and (2) demonstrates that only two variants are possible:

a) $\lambda_1, \lambda_2 \neq 0$, $\lambda_3 = \lambda_4 = 0$. Polarizations $s_{p1}(t)$ and $s_{p2}(t)$ should be mutually orthogonal and $p = 0$ for all h satisfying the condition $|h_1|^2/|h_2|^2 = \langle|t_{22}|^2\rangle(\langle|t_{11}|^2\rangle)^{-1}$, (which corresponds to a certain circle ℓ in fig 1).

b) $\lambda_3, \lambda_4 \neq 0$, $\lambda_1 = \lambda_2 = 0$.

Polarization $s_{p3}(t)$ and $s_{p4}(t)$ are non-orthogonal and $p = 0$ with $h = e_1$ and $h = e_2$.

3. Let us assume that three λ_i differ from zero (λ_r, λ_m, $\lambda_n \neq 0$; $r,m,n = \overline{1,4}$). From (1) and (2) it follows that the equality $p = 0$ can be obtained with no more than two values of h. One of the possible variants is shown in fig 2: $\lambda_4 = 0$; $\lambda_1,\lambda_2,\lambda_3 \neq 0$. Equality $p = 0$ is fulfilled with $\lambda_2/\lambda_1 = |h_1|^2/|h_2|^2$ and $\cos\alpha = 0$, i.e., at point C_1 and C_2 ($\lambda_2 > \lambda_1$). With $\lambda_1 = \lambda_2$, $p = 0$ for circular polarizations, points R and L.

4. Let us assume that all λ_i differ from zero. Let us note that by the selection of the appropriate values of h it is possible to achieve the equality to zero of the intensities of three waves simultaneously ($J_{p1(2)} = J_{p3} = J_{p4} = 0$ with $|h_{1(2)}| = 0$) or the intensity of a single wave ($J_{p3(4)} = 0$ with $\cos\alpha$ ($\sin\alpha$) $= 0$). In the first case $p \neq 0$; in the second $p = 0$ only with a definite relationship between the polarizations and intensities of the remaining waves. Fig 3a illustrates the case when the polarized component of the wave, $s_{12}(t) = s_{p1}(t) + s_{p2}(t)$, is

orthogonal to the polarization, $s_{p3}(t)$; the intensities are equal and $J_{p4} = 0$. It is not difficult to note that this is possible only with a certain single value of h . In the case when all $J_{pj} \neq 0$, $j = 1,4$, equality $p = 0$ also can be fulfilled for a certain RLTs. Fig 3b corresponds to the case when the polarized components of the wave, $s_{12}(t) = s_{p1}(t) + s_{p2}(t)$ and $s_{34}(t) = s_{p3}(t) + s_{p4}(t)$, are mutually orthogonal and their intensities are equal. From (1) and (2) it is obvious that this can be realized for only a certain single value of h .

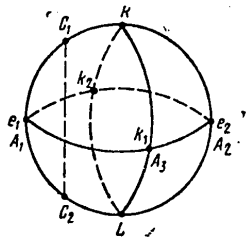

Figure 2.

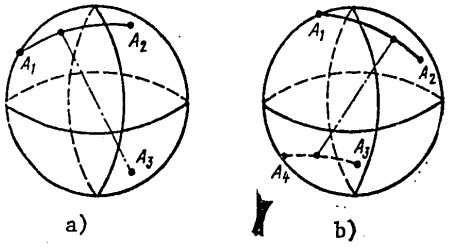

Figure 3.

Thus, for a fluctuating RLTs with a symmetric random scattering matrix it is possible to obtain chaotically polarized reflected signals for one of the following three sets of RLS radiation polarizations: 1) for single polarization; 2) for two polarizations; 3) for a set of polarizations to which on a Poincaré sphere corresponds a certain circle.

Bibliography

1. Kanareykin, D.B., Potekhin, V.A. and Shishkin, I.F. "Morskaya polyarimetriya" [Marine Polarimetry], Leningrad, Sudostroyeniye, 1968.

2. Pozdnyak, S.I. and Melititskiy, V.A. "Vvedeniye v statisticheskuyu teoriyu polyarizatsii radiovoln" [Introduction to the Statistical Theory of the Polarization of Radio Waves], Moscow, Sovetskoye Radio, 1974.

3. Zhivotovskiy, L.A. RADIOTEKHNIKA, Vol 31, No 12, 1976.

4. Zhivotovskiy, L.A. RADIOTEKHNIKA I ELEKTRONIKA, Vol 17, No 10, 1972.

8831
CSO: 1860

UDC 621.396.9

DOPPLER FILTRATION IN HF DIRECTION-FINDING IN COMBINATION WITH A METHOD OF ANALYTIC BEAM SEPARATION

Moscow RADIOTEKHNIKA I ELEKTRONIKA in Russian No 8, 1979
pp 1558-1563

[Article by Yu. M. Agafonnikov, E. L. Afraymovich and V. P. Polimatidi]

[Text] This presents a synthesis of the method of Doppler filtration and the analytic separation of the components in a multimode HF radio signal. The combined method possesses an enhanced resolution capability and interference immunity, and may find application both in ionospheric diagnostics using low-powered continuous signals, as well as in practical radio direction-finding.

1. Doppler Separation

The operation of classical HF radio direction-finding equipment under multimode wave field conditions is characterized by great interference errors. Lately there has appeared a series of works devoted to the development and testing of a direction-finder with Doppler filtration (separation) of the components [1-4]. The feasibility of such separation is insured by the difference in the Doppler shift of frequencies in those modes which diffuse in the ionosphere along various trajectories (experiment [3-6], calculations [6,7]). The processing of the signal is carried out through numerical or analog-digital means in accordance with the following procedures (the simplest version is [1-4]).

1. Recording the complex amplitude $\tilde{U}(t)_{x,y}$ of one of the projections of the field of the HF radio signal over the time interval T at points M (M=2 or 3) distributed in space along the coordinates $\{x_m, y_m\}$; m=1,2,...,M. For a regular type multimode signal in the first approximation it is possible to write

$$(1) \qquad U(t)=\sum_{j=1}^{N} r_j \exp(-i(2\pi f_j t-u_j x-v_j y+\varphi_j)),$$

$$(2) \qquad u_j=\frac{2\pi}{\lambda}\cos\theta_j \sin\psi_j, \quad v_j=\frac{2\pi}{\lambda}\cos\theta_j\cos\psi_j,$$

where r_j is the amplitude; f_j is the Doppler shift; Φ_j is the phase; θ_j is the elevation; Ψ_j is the azimuth of the j component of the multimode field; and λ is the wavelength. For convenience we will write also

$$(3) \qquad \operatorname{tg}\psi_j=\frac{u_j}{v_j}, \quad \cos\theta_j=\frac{\lambda}{2\pi}\sqrt{u_j^2+v_j^2}.$$

2. A complex Fourier transformation for solving $\tilde{U}(t)_{x,y}$:

$$(4) \qquad \tilde{S}(\omega)_{x,y}=S(\omega)e^{i\Phi(\omega)}=\int_{\tau} U(t)_{x,y}e^{-i\omega t}dt; \quad \omega=2\pi f,$$

where $S(\omega)$ and $\Phi(\omega)$ are the amplitude and phase spectra.

3. Computation of the angles $\Psi(\omega)$ and $\theta(\omega)$ for all spectral components according to formulae (3) with the substitution

$$(5) \qquad v(\omega)=\frac{\Delta\Phi_x(\omega)}{d_x}, \quad u(\omega)=\frac{\Delta\Phi_y(\omega)}{d_y},$$

where $\Delta\Phi_{x,y}(\omega)$ is the phase difference and d_x and d_y is the separation (base line) between antennas.

4. The construction of a weighted distribution according to the magnitude of the spectral components along the angles of arrival (a secondary treatment).

The Doppler filtration not only makes possible the elimination, basically, of the interference error but also insures high interference immunity in measuring the arrival angles (equivalent to a single-filter band of approximately 0.01-0.1 Hz).

The given method makes it possible to separate the k and l-components of a multimode radio wave for which the Doppler shift in frequency is

$$|f_k - f_l| > 1/T.$$

Under normal ionospheric conditions T on the order of 10-100 seconds is sufficient for successfully separating the components [1-5]. An obstacle to a successful solution with this method (for increased T) is the transient nature of ionospheric processes; the time constant for changes in the Doppler shift in frequency is on the order of 1-5 min. Even more important in problems of practical radio direction-finding are the time constraints on the operation of the transmitter. For unsolved components the interference error can be substantial; in the one-dimensional case the calculated angle of arrival

$$\sin\theta_{\text{изм}} = \frac{r_k^2 \sin\theta_k + r_l^2 \sin\theta_l + r_k r_l (\sin\theta_k + \sin\theta_l)\cos(\Delta\varphi)}{r_k^2 + r_l^2 + 2 r_k r_l \cos(\Delta\varphi)}$$

depends upon the amplitude, the arrival angles and the phase difference of the k and l-components.

2. Analytic Separation

We will now examine the other possibility of separating the components of a multimode field, worked out in [8-11]. For a fixed moment in time we transform (1) into

$$U(x, y) = \sum_{j=1}^{N} \tilde{A}_j \exp(-i(u_j x + v_j y)), \tag{6}$$

where $\tilde{A}_j = r_j \exp(-i\Phi_j)$.

Expression (6), written for a bank of spatially dispersed antennas, forms a system of transcendental equations relating to the unknowns r_j, Φ_j, v_j, u_j. Obviously, at least 2N antennas are required for the determination of the stated parameters of N waves.

For simplicity's sake we will examine the case when N=2 and assume that antennas 1, 2, 3, 4 are arranged at the vertices of a square of side a ($x_1=y_1=y_2=x_3=0$; $x_2=y_3=x_4=y_4=a$) [9], then

$$\begin{cases} U_1 = \tilde{A}_1 + \tilde{A}_2, \\ U_2 = \tilde{A}_1 \exp(-iau_1) + \tilde{A}_2 \exp(-iau_2), \\ U_3 = \tilde{A}_1 \exp(-iav_1) + \tilde{A}_2 \exp(-iav_2), \\ U_4 = \tilde{A}_1 \exp(-ia(u_1+v_1)) + \tilde{A}_2 \exp(-ia(u_2+v_2)). \end{cases} \tag{7}$$

We are interested in the solution to the system (7) with reference to the parameters u,v,A. From the two upper equations it follows that

$$A_1=\frac{U_1\exp(-iau_2)-U_2}{\exp(-iau_2)-\exp(-iau_1)}, \tag{8a}$$

$$A_2=\frac{U_2-U_1\exp(-iau_1)}{\exp(-iau_2)-\exp(-iau_1)}, \tag{8b}$$

and from the lower two

$$A_1=\frac{U_3\exp(-iau_2)-U_4}{(\exp(-iau_2)-\exp(-iau_1))}\exp(iav_1), \tag{8c}$$

$$A_2=\frac{U_4-U_3\exp(-iau_1)}{(\exp(-iau_2)-\exp(-iau_1))}\exp(iav_2). \tag{8d}$$

Combining (8a) with (8c) and also (8b) with (8d) we get

$$\frac{U_1\exp(-iau_1)-U_2}{U_3\exp(-iau_1)-U_4}\exp(-iav_2)=1, \tag{9a}$$

$$\frac{U_1\exp(-iau_2)-U_2}{U_3\exp(-iau_2)-U_4}\exp(-iav_1)=1. \tag{9b}$$

The left parts of equations (9a) and (9b) are complex expressions, the absolute value of which is equal to unity and the argument is equal to zero. Taking into consideration that $|\exp(-iav_{1,2})|=1$, for $u_{1,2}$ we obtain the equation

$$\left|\frac{U_1\exp(-iau_{1,2})-U_2}{U_3\exp(-iau_{1,2})-U_4}\right|=1. \tag{10}$$

The last equation transforms to

$$D\cos(au_{1,2}+C)=B, \tag{11}$$

where $D=\sqrt{(R_1R_2)^2+(R_3R_4)^2-2R_1R_2R_3R_4\cos(\Phi_{43}-\Phi_{21})}$;

$$\operatorname{tg}C=\frac{R_1R_2\cos\Phi_{21}-R_3R_4\cos\Phi_{43}}{-R_1R_2\sin\Phi_{21}-R_3R_4\sin\Phi_{43}}.$$

$B=(R_1^2+R_2^2-R_3^2-R_4^2)/2$;

$U_j=R_j\exp(i\Phi_j)$; $\Phi_{jk}=\Phi_j-\Phi_k$.

After $u_{1,2}$ are derived from (11) equations (9a) and (9b) are solved relative to $v_{2,1}$ and $\tilde{A}_1$ and $\tilde{A}_2$ are determined from (8a) and (8b).

Thus, in the presence of two waves a unique solution can be found using the instantaneous amplitude and phase of the potentials induced by the interference field at four spatially dispersed points.

If a single wave field acts upon this system of antennas, then it turns out that D=B=0. Thus, the solution cannot be found in the form of (11) and it must be sought in the first three equations of system (7).

If N>2, such relations as R_j, Φ_j, (j=1,2,3,4) are possible where B>D. Thus, no two-wave solutions exist. This inequality may serve as one of the criteria of a situation in which the measured interference field is composed of a greater number of waves than the order of magnitude of the applied solution. The physical soundness of the results obtained usually serves as a practical criterion for the presence of a greater number of waves, for example, when there is an absence of any significant variation in the results.

The simultaneous equations of type (7) for N>2 cannot be reduced to a simple equation. Thus, for N=3 we have

$$(12)\quad \begin{aligned} &\frac{(U_1\exp(-iav_1)-U_3)\exp(-iav_2)-(U_3\exp(-iav_1)-U_5)}{(U_2\exp(-iav_1)-U_4)\exp(-iav_2)-(U_4\exp(-iav_1)-U_6)}\times\\ &\times e^{-iau_2}=1,\\ &\frac{(U_1\exp(-iav_2)-U_3)\exp(-iav_3)-(U_3\exp(-iav_2)-U_5)}{(U_2\exp(-iav_2)-U_4)\exp(-iav_3)-(U_4\exp(-iav_2)-U_6)}\times\\ &\times e^{-iau_1}=1,\\ &\frac{(U_1\exp(iav_3)-U_3)\exp(-iav_1)-(U_3\exp(-iav_3)-U_5)}{(U_2\exp(-iav_3)-U_4)\exp(-iav_1)-(U_4\exp(-iav_3)-U_6)}\times\\ &\times e^{-iau_3}=1. \end{aligned}$$

Thus, we undertake other methods of deriving an analytic solution. Redundant information is usually used for this-a number of required antennas greater than 2N. Therefore, in [10] the proposed method leads to linear simultaneous equations in which, for the cases 2K and (2K+1) waves, 5K and (5K+3) antennas, respectively, are required. The use of this method makes it possible to find only the vertical angles of arrival, assuming that the azimuth angles of the various waves are coincident.

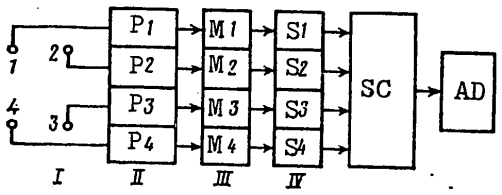

Fig. 1

I - recording of the field at transducers distributed in space; II - multichannel coherent pickup; III - measurement of the complex amplitude; IV - spectroanalyzer; SC - special computer for calculating the wave parameters of each of the spectral components; AD - analysis and display of the information.

There is another analytic method for separating the waves in which the number of antennas can be <2N [11]. With this method, assuming that each of the interfering waves has a constant frequency shift with respect to time (for the interval of analysis), equations can be written for an interference field about spatially-distributed points for a sequence of equally-spaced time intervals.

In such a manner, the analytic method essentially makes it possible to separate the waves comprising a multimode field and to compute separately their parameters for instantaneous values of the field's complex amplitude. There are, however, several factors which limit the feasibility of the method. One of these is related to the fact that this method is analytic, and in the presence of interference an instability appears in the analytic solutions which grows with increases in N. A second factor is related to the increase in the number of required antennas as N grows larger, accompanied by increased limitations on the time of measurement. We will note that the interference resistance of the method is determined by the radio bandwidth, which, in the given case, should not be less than $(f_{max}-f_{min})$, where f_{max} and f_{min} are the maximum and minumum Doppler shifts in the frequency of the interfering waves.

3. The Combined Method

The authors have suggested a synthesis of the Doppler and analytic separations, which makes it possible to enjoy the advantages of both methods and, to a significant degree, to compensate for their shortcomings [12]. The essence of the procedure consists of first performing the operations which provide the

Doppler separation (see above). In this method, the components for which $\Delta f > 1/T$ are successfully filtered out. For eliminating the residual noise in those components worthy of attention (that is, of sufficient amplitude) they solve simultaneous equations of type (6), as in the method of analytic separation. This is done not to solve for the instantaneous values of the complex amplitudes of the field $\tilde{U}(x,y)$, but for the complex spectral amplitudes $\tilde{S}(\omega)_{x,y}$ of the selected frequency ω.

Allowing for prior Doppler filtration, it can be assumed that in the selected ω-filter no more than two components are interfering. This requires four antennas, which is only one more antenna than would be necessary in the most minimal configuration for a direction-finder's antenna array. With the arrangement of antennas chosen in Part 2, the solution to the simultaneous equations relative to parameters u,v can be obtained from the relations

$$\begin{aligned}&\frac{\mathcal{S}_1(\omega)\exp(-iau_1)-\mathcal{S}_2(\omega)}{\mathcal{S}_3(\omega)\exp(-iau_1)-\mathcal{S}_4(\omega)}\exp(-iav_2)=1,\\&\frac{\mathcal{S}_1(\omega)\exp(-iau_2)-\mathcal{S}_2(\omega)}{\mathcal{S}_3(\omega)\exp(-iau_2)-\mathcal{S}_4(\omega)}\exp(-iav_1)=1.\end{aligned}\tag{13}$$

The sequence of operations is depicted in fig. 1.

As an example we will examine a typical Doppler spectrum of a reflected HF signal of 7336 kHz on a medium-width route of 4100 km [5] (fig. 2). The spectrum is obtained using a time factor T=40 sec, Δf=0.025 Hz. In this case, for the application of the suggested method to determine the parameters of five interfering modes (N=5) the width of the spectral line is 0.025 Hz; solutions for the modes in the spectral lines were not derived for two modes, thus M=2. When utilizing a multiwave direction-finder that measures the parameters according to instantaneous readings, the signal has to be received in a frequency band $\Delta F \geq 1.5$ Hz. The resultant gain in the frequency band is not less than $\Delta F/\Delta f$=60 times. The number of transducers employed decreases from 10 to 4.

The essential feature is not only the reduction of the series in system (6) as a result of prior Doppler filtration and, correspondingly, a decrease in the number of antennas and a simplification in the computational aspect of processing the signal. No less important is the sharp increase in interference

immunity of the measurement, provided that the latter is determined now by the value $\Delta f=1/T\ll(f_{max}-f_{min})$. The stability of the system's solution in (13) is also much greater than the stability of the system's solution in (9), since (9) is solved relative to the instantaneous values of the complex amplitudes $\tilde{U}(x,y)_t$, while (13) is solved relative to the complex spectral amplitudes $\tilde{S}(\omega)_{x,y}$ derived from integration over a sufficiently large interval T (approximately 1000 readings $\tilde{U}(x,y)_t$).

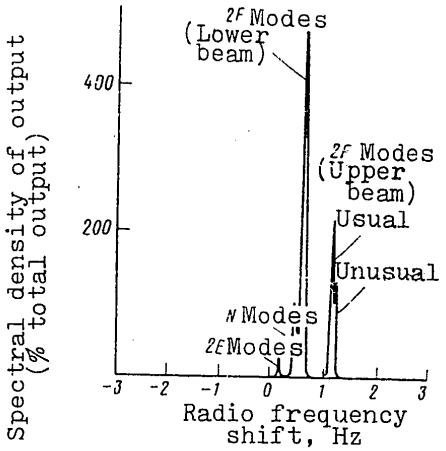

Fig. 2

The possibility of achieving as analytic separation of the modes in addition to the Doppler separation permits shortening the time of analysis to a value of ~10-20 sec, which is particularly important in practical applications and in investigations of the non-stationary ionosphere.

The authors are grateful to L. A. Lobachevskiy, V. S. Lobachevskaya and I. S. Volginaya for their constant attention and assistance in this work.

BIBLIOGRAPHY

1. Afraymovich, E. L., et al. In "Issledovanya po geomagnetizmu, aeronomii i fizike colntsa" [Investigations of the Geomagnetism, Aeronomy and Physics of the Sun], Vyp's 32, 33, 41, No's 33, 55, 50, Moscow, Nauka, 1974, 1975, 1977.

2. Bennet, S. M. US Patent, N 3991. 418, Nov 9, 1976.

3. Afraymovich, E. L. RADIOTEKHNIKA I ELEKTRONIKA, Vol 24, No 7, 1979, p 1444.

4. Afraymovich, E. L., and Panchenko, V. A. "Dopplerovskaya fil'tratsiya v KV-pelengatsii. Analogo-tsifrovaya obrabotka modulirovannogo signala" [Doppler Filtration in HF Direction-finding. An Analog-numeric Treatment of the Modulated Signal], IZMIRAN SSSR, No 18, 1978, p 217.

5. Shepard, R. A., and Jomax, J. B. IEEE TRANS. COM. TECHNOL., COM-15, No 2, 1967, p 268.

6. Bayuklina, M. F., and Krasnov, V. M. In "Teoreticheskoe i eksperimental'noe issledovanie rasprostraneniya dekametrovykh radiovoln" [Theoretical and Experimental Investigation of Decimetric Radio Waves]. Moscow, IZMIRAN SSSR, 1976, p 73.

7. Boldovskaya, I. G. GEOMAGNETIZM I AERONOMIYA, Vol 19, No 2, 1979, p 251.

8. Kukes, I. S., and Starik, M. E. "Osnovy radiopelengatsii" [Principles of Radio Direction-finding]. Izd. Sovetskoe radio, 1964.

9. Baur, K. FREQUENZ, Vol 14, No 2, 1960, p 41.

10. Kelso, J. M. RADIO SCI., Vol 7, No 2, 1972, p 245.

11. Baur, K. Bundesrepublik deutschland, Patentschritt N 2328720, 2.10.1975.

12. Agafonnikov, Yu. M.; Afraymovich, E. L.; and Polimatidi, V. P. "A Method of Measuring the Parameters of a Multimode Wave Field," in "Otkrytiya, izobreteniya, promyshlennye obraztsy, tovarnye znaki" [Discoveries, Inventions, Industrial Designs] Authors License No 652489, Vol 10, 1979, p 172.

[23-9512]

9512
CSO: 1860

UDC 621.396.96.06

DISTORTIONS OF THE RADAR CHARACTERISTICS OF COMPLEX OBJECTS WHEN EXPOSED TO A SPHERICAL WAVE

Moscow RADIOTEKHNIKA in Russian No 10, 1979 pp 67-69 manuscript received after completion 9 Jan 79

[Article by V.M. Shlyakhin]

[Text] A key objective in the further development of equipment for measuring the radar characteristics (RLKh's) of objects in models is the development of a procedure for estimating and taking into account measurement errors [1]. For this purpose, in this study an analysis is made of distortions of the statistical RLKh's of complex objects, representing a random combination of interconnected reflectors, when exposed to a spherical wave.

Let there fall onto a system of interconnected reflectors (fig 1) a wave spherical in terms of phase with a radius of curvature of its front of R_0. Representing the field scattered by a complex object when exposed to a spherical wave as the result of the superposition of fields scattered by each elementary reflector, we determine

$$E_{\Sigma}^{0} = \sum_{n=1}^{N} \sqrt{\sigma_n(\alpha)}\, e^{i\left[2kr_n \sin(\alpha+\varphi_n) + 2\psi_n \cos^2(\alpha+\varphi_n) + \beta_n(\alpha)\right]}, \tag{1}$$

where $\sigma_n(\alpha)$ is the monostatic diagram of the secondary radiating element of the n-th reflector; $\beta_n(\alpha)$ is the phase diagram of the n-th reflector; N is the number of reflectors; and r_n and ϕ_n are the geometrical characteristics of the system of reflectors; and $\psi_n = kr_n^2/2R_0$.

If the linear dimensions of each n-th reflector are small as compared with R_0, then the wave striking it is locally plane, and characteristics $\sigma_n(\alpha)$ and $\beta_n(\alpha)$ do not differ from the corresponding characteristics of reflectors in exposure to a plane wave.

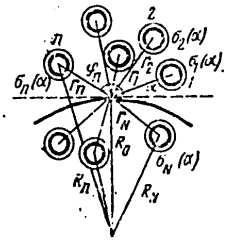

Figure 1.

Since under real conditions the signal scattered by a target is of a random nature, in processing the results of measurements of the RLKh's of objects in models, the angle of the radiation, α, is assumed to be random and statistical RLKh's are computed. We will assume that the distribution law for random parameter α is given by the equation

$$W(a) = \frac{\exp[d\cos(a_0 - a)]}{2\gamma_0 I_0(d)}, \quad \gamma_0 \leqslant \pi, \tag{2}$$

where γ_0 is the averaging interval, $I_0(d)$ is a modified Bessel function, and α_0 and d are characteristics of the mean value and the variance of random parameter α.

In investigations of the RLKh's of objects one is usually interested in their averaged values over the entire possible range of angles of exposure ($-\pi$ to $+\pi$) or in a fairly narrow sector in relation to the selected direction. Therefore we will restrict ourselves to discussing two practically important cases: $\gamma_0 = \pi$ and $\gamma_0 \leq 0.1\pi$.

From (1) it follows that with random parameter α the quadrature components of the harmonic signal, $z(t) = \mathrm{Re}\{E_\Sigma^0 e^{j\omega t}\}$, scattered by a system of reflectors in exposure to a spherical wave, are also random. Furthermore,

$$\left.\begin{aligned} x^0 - x^\Pi &= -2\sum_{n=1}^{N}\sqrt{\sigma_n(\alpha)}\sin(\psi_n\cos^2\alpha_n)\sin[2kr_n\sin\alpha_n + \psi_n\cos^2\alpha_n + \beta_n(\alpha)], \\ y^0 - y^\Pi &= 2\sum_{n=1}^{N}\sqrt{\sigma_n(\alpha)}\sin(\psi_n\cos^2\alpha_n)\cos[2kr_n\sin\alpha_n + \psi_n\cos^2\alpha_n + \beta_n(\alpha)], \end{aligned}\right\} \tag{3}$$

where x^0, y^0, x^p and y^p are the quadrature components of a signal scattered by a combination of reflectors in exposure to a spherical and plane wave, and $\alpha_n = \alpha + \phi_n$.

With a sufficiently great number of reflectors, according to the conditions of the central limit theorem, the distribution law for random values x^0 and y^0 is asymptotically normal with a mathematical expectation of

$$\langle x^0 \rangle = \sum_{n=1}^{N} \langle x_n^0 \rangle, \quad \langle y^0 \rangle = \sum_{n=1}^{N} \langle y_n^0 \rangle$$

and a variance of

$$D\{x^0\} = \sum_{n=1}^{N} D\{x_n^0\}, \quad D\{y^0\} = \sum_{n=1}^{N} D\{y_n^0\}.$$

Averging (3) in keeping with (2), we determine that generally $\langle x^0 \rangle \neq \langle x^p \rangle \neq \langle y^0 \rangle \neq \langle y^p \rangle$ and $D\{x^0\} \neq D\{x^p\} \neq D\{y^0\}$. For example,

$$\begin{aligned}
\langle x_n^0 \rangle &\simeq \langle \sqrt{\sigma_n(\alpha)} \rangle \cos\psi_n \{J_0(\sqrt{b}) \langle \cos[\psi_n + \beta_n(\alpha)] \rangle - J_2(\sqrt{b}) \operatorname{tg}\psi_n \langle \sin[\psi_n + \beta_n(\alpha)] \rangle\};\\
\langle y_n^0 \rangle &\simeq \langle \sqrt{\sigma_n(\alpha)} \rangle \cos\psi_n \{J_0(\sqrt{b}) \langle \sin[\psi_n + \beta_n(\alpha)] \rangle + J_2(\sqrt{b}) \operatorname{tg}\psi_n \langle \cos[\psi_n + \beta_n(\alpha)] \rangle\}, \quad \gamma_0 = \pi;\\
\langle x_n^0 \rangle &\simeq \langle \sqrt{\sigma_n(\alpha)} \rangle \cos\psi_n \sin C(2kr_n\gamma_0) \{\langle \cos[\psi_n + \beta_n(\alpha)] \rangle - \operatorname{tg}\psi_n \langle \sin[\psi_n + \beta_n(\alpha)] \rangle\}, \quad \gamma_0 \leqslant 0,1\pi,
\end{aligned} \tag{4}$$

where $J_m(x)$ is a Bessel function; $b = 4k^2r_n^2 - d^2$; and $\sin C_x = \sin x/x$.

From this it is obvious that the curvature of the front of the irradiated wave ($\psi_n \neq 0$) results in intensification of differences between like characteristics of the signal's quadrature components. In addition, it follows from (4) that with wide averaging intervals the error in measuring statistical characteristics of a signal's quadrature components increases with a reduction in the value of $4k^2r^2 - d^2$. Therefore, with $kr_n = \text{const}$ and a uniform distribution of α ($d^n = 0$), the error in measuring these characteristics is minimal as compared with other distribution laws for a random angle of exposure ($d > 1$). With reduction of the averaging interval to $\gamma_0 \leq 0.1\pi$, the differences between characteristics of quadrature components are intensified and there is an increase (of approximately an order of magnitude) in the error in measuring these characteristics, caused by curvature of the front of the irradiating wave. But, if the distances between reflectors (in wavelengths) are greater than the inverse value of the averaging interval,

$$\left[\text{or } r_n/\lambda \geqslant \frac{1}{4\gamma_0 \cos(\alpha_0+\varphi_n)} + \frac{\psi_n}{\pi}\sin(\alpha_0+\varphi_n) \;;\; \alpha_0+\varphi_n \neq 0\right],$$

the statistical characteristics of the signal's quadrature components practically do not depend on the radius of the front of the irradiating wave.

Reasoning in a similar manner, it is possible to demonstrate that the intercorrelation coefficient between components, $R\{x^0,y^0\}$, generally is not equal to zero and also depends on the radius of the front of the irradiating wave.

Taking the above into account, we establish that generally the statistical structure of the signal scattered by a combination of interconnected reflectors in exposure to a spherical wave is described by a generalized probabilistic model of the envelope and phase of random signals [2,4]. For practical calculations it is more convenient to use another type of approximation of the real distribution of the amplitude of random signals--the Nakagami distribution:*

$$W\left(\frac{A}{\sigma_\Sigma}\right) = \frac{2}{\Gamma(m)}\left(\frac{A^{2m-1}}{\sigma_\Sigma^{m-1}}\right)\exp\left\{-\frac{m}{\Omega}A^2\right\}\left\{-\frac{m}{\Omega}\sigma_\Sigma\right\}, \tag{5}$$

where A is the amplitude of the signal, σ_Σ is the effective scattering surface (EPR) of the object and $\Gamma(m)$ is a gamma function.

Utilizing the results of [2-4], it is not difficult to establish the relationship between the distribution parameters in (5) and characteristics of quadrature components x^0 and y^0 and at the same time to determine their dependence on the geometrical characteristics of the system of reflectors and the radius of the front of the irradiating wave.

By employing statistical methods, it is possible to estimate also the error in measuring instantaneous values of the characteristics of a signal scattered by a complex object when exposed to a spherical wave [5].

Conclusions

1. The statistical structure of a signal scattered by a combination of interconnected reflectors when exposed to a spherical wave is described by a generalized probabilistic model of the envelope (amplitude) and phase of random signals.

*Probability density $W(\sigma_\Sigma)$ is determined in (5) with an accuracy of a constant.

2. Curvature of the front of the irradiating wave results in the intensification of differences between like characteristics of quadrature components of the scattered signal.

3. With an increase in distances between reflectors (in wavelengths) to $r_n/\lambda >> (1 + d)$, $\gamma_0 = \pi$ and $r_n/\lambda \gtrsim [1/4\gamma_0 \cos(\alpha_0 + \phi_n)]$, $\gamma_0 \leq 0.1\pi$ (d and α_0 are the distribution parameters of the random angle), the statistical RLKh's of a complex scatterer are determined only by the properties of elementary reflectors and practically do not depend on the radius of the front of the irradiating wave.

Bibliography

1. Mayzel's, Ye.N. and Torgovanov, V.A. "Izmereniye kharakteristik rasseyaniya radiolokatsionnykh tseley" [Measurement of the Scattering Characteristics of Radar Targets], Moscow, Sovetskoye Radio, 1972.

2. Pozdnyak, S.I. and Melititskiy, V.A. "Vvedeniye v statisticheskuyu teoriyu polyarizatsii radiovoln" [Introduction to the Statistical Theory of the Polarization of Radio Waves], Moscow, Sovetskoye Radio, 1974.

3. Nakagami, M. "The m-Distribution--a General Formula of Intensity Distribution of Rapid Fadings" in "Statistical Methods in Radio Wave Propagation," Pergamon Press, 1960.

4. Beckmann, P. and Spizzichino, A. "The Scattering of Electromagnetic Waves from Rough Surfaces," Pergamon Press, Oxford-London-New York-Paris, 1963.

5. Kuznetsov, Yu.A., Melititskiy, V.A. and Shlyakhin, V.M. RADIOTEKHNIKA, Vol 33, No 12, 1978.

[59-8831]

8831
CSO: 1860

UDC 621.396.96:621.391.26

SYNTHESIS OF A SINGLE-PULSE DISCRIMINATOR FOR A LOCATED TARGET

Moscow RADIOTEKHNIKA I ELEKTRONIKA in Russian Vol 24 No 4, 1979 manuscript received 29 Mar 77 pp 852-854

[Article by N. Ya. Kuz']

[Text] Various methods can be used to increase the angular resolution of a monopulse radar [1, 2]. One of them is based on the use of angular strobing which permits the corresponding coarsening or complete shutdown of the tracking system automatically with the presence of several targets in the resolved volume or when there is flickering noise.

The data on the composition (nature) of a located target (single or group), required to control the strobing device, can be obtained by different methods. For example, a method based on creation of an energy contrast of targets by using two transmitting and two receiving devices, is considered in [4]. Besides the complexity, a significant disadvantage of the given method is the low efficiency when operating, for example, in the passive mode by radiation sources. In this regard it is of interest to determine methods of distinguishing the composition of the located target which follow directly from statistical decision theory.

Let us limit ourselves to consideration of the two-dimensional case, assuming that signal reception is accomplished by two antennas, the radiation patterns $F_1(\alpha)$ and $F_2(\alpha)$ of which are shown in Figure 1. Let us assume that signal $\xi(t)$ received from angular direction α_1, read from an equisignal, corresponds to hypothesis H1 and that mutually uncorrelated signals $\xi_1(t)$ and $\xi_2(t)$ received from directions $\alpha_1 - \delta\alpha$ and $\alpha_1 + \delta\alpha$, respectively, correspond to hypothesis H_2.

Bearing in mind the relatively small values of α_1 and $\delta\alpha$, let us represent the radiation patterns $F_1(\alpha)$ and $F_2(\alpha)$ in the form

$$F_1(\alpha) \approx r - k\alpha, \quad F_2(\alpha) \approx r + k\alpha,$$

where $r = F_1(0) = F_2(0)$; $k = (d/d\alpha) F_2(\alpha)_{\alpha=0}$.

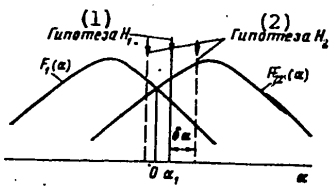

Figure 1

Key:
1. Hypothesis H_1 2. Hypothesis H_2

Then at the outputs of the first and second antennas we will have, respectively,

a) for hypothesis H_1:

$$x_1(t)=n_1(t)+\xi(t)\,(r-k\alpha_1),\quad x_2(t)=n_2(t)+\xi(t)\,(r+k\alpha_1), \tag{1}$$

b) for hypothesis H_2:

$$x_1(t)=n_1(t)+\xi_1(t)\,(r-k\alpha_1+k\delta\alpha)+\xi_2(t)\,(r-k\alpha_1-k\delta\alpha),$$

$$x_2(t)=n_2(t)+\xi_1(t)\,(r+k\alpha_1-k\delta\alpha)+\xi_2(t)\,(r+k\alpha_1+k\delta\alpha). \tag{2}$$

Here $n_1(t)$ and $n_2(t)$ are the mutually uncorrelated thermal noise which we will regard as "white" noise and which has identical spectral output density N_0.

Let us assume that the signal output $\xi(t)$ is equal to the total signal output $\xi_1(t)$ and $\xi_2(t)$. Let us also assume that the frequency structure ("the tint") of signals $\xi(t)$ and $\xi_{1(2)}(t)$ is identical so that some features of their discrimination are absent at $\delta\alpha = 0$. In this case the matrices of the cross-correlated functions of signals corresponding to the antenna outputs can be represented in the form

a) for hypothesis H_1:

$$\mathbb{K}_1(t, s)=N_0\mathrm{I}\delta(t-s)+b(t, s)\,\psi\psi^{\mathrm{T}},$$

b) for hypothesis H_2:

$$\mathbf{K}_2(t, s)=N_0\mathrm{I}\delta(t-s)+b(t, s)\,[\psi\psi^{\mathrm{T}}+(k\delta\alpha)^2\mathbf{g}\mathbf{g}^{\mathrm{T}}],$$

where I is the unit matrix and ψ and g are two-dimensional column vectors:

$$\psi = \begin{pmatrix} r-k\alpha_1 \\ r+k\alpha_1 \end{pmatrix}, \quad g = \begin{pmatrix} 1 \\ -1 \end{pmatrix};$$

$$b(t, s) = \overline{\xi(t)\xi(s)} = (1/2)\overline{\xi_1(t)\xi_1(t)} = (1/2)\overline{\xi_2(t)\xi_2(t)}.$$

As in [3], let us reduce the considered signal discrimination problem to one of detection and let us use the rather well-developed mathematical apparatus for solving it. For this purpose, we shall assume that the correlation matrix $K_1(t, s)$ is a noise matrix and we shall introduce the following correlation matrix for the useful signal

$$K_c(t, s) = K_2(t, s) - K_1(t, s) = b(t, s)(k\delta\alpha)^2 gg^T.$$

Let us limit ourselves to consideration of the case of gaussian signals important to practice. The adequate test statistics may then be represented in the form of the quadratic functional

$$L = \iint_T X^T(t) V(t, s) X(s)\, dt\, ds, \tag{3}$$

where $X^t(t)$ is the row vector of signals to be processed in the range of $t \in T$, $X^t(t) = x_1(t)x_2(t))$ and V(t, s) is a matrix determined from the integral equations

$$\int_T V(t, s) K_2(s, \tau)\, ds = \int_T W(t, s) K_1(s, \tau)\, ds, \tag{4}$$

$$\int_T W(t, s) K_1(s, \tau)\, ds = I\delta(t-\tau). \tag{5}$$

Let us assume for definiteness that the discriminated signals are noisy and they have uniform energy spectra in the frequency band Π ($\pi T \gg 1$) such that b(t, s) = N sin $[\pi \Pi (t - s)]/\pi (t - s)$. Solving integral equations (5) and (4), we find in this case

$$V(t, s) = \eta D g g^T D \sin [\pi\Pi(t-s)]/\pi(t-s), \tag{6}$$

where D is a matrix inverse to the matrix $I + (N/N_0)\psi\psi^t$ and η is the scalar coefficient.

Substitution of the right side of (6) into (3) yields

$$L=\eta\int_T\left[\int_T\frac{\sin[\pi\Pi(t-s)]}{\pi(t-s)}w(s)\,ds\right]^2 dt, \tag{7}$$

where w(s) is the scalar signal and

Let us represent in explicit form the scalar signal w(t) contained in the subintegral equation (7). Noting that $\mathbf{D}=\mathbf{I}-N\psi\psi^T/(N_0+\psi^T\psi)$, $\mathbf{Dg}=\mathbf{g}-N\psi^T\mathbf{g}\psi/(N_0+N\psi^T\psi)$, $\psi^T\mathbf{g}=-2k\alpha_1$, $\psi^T\psi=2(r^2+k^2\alpha_1^2)$, we find

$$w(t)=\mathbf{X}^T(t)\mathbf{g}+\frac{2Nk\alpha_1\mathbf{X}^T(t)\psi}{N_0+2N(r^2+k^2\alpha_1^2)}.$$

In turn $\mathbf{X}^T(t)\mathbf{g}=-x_\Delta(t)$, $\mathbf{X}^T(t)\psi=k\alpha_1 x_\Sigma(t)+rx_\Sigma(t)$, where $x_\Delta(t)$ and $x_\Sigma(t)$ are the difference and total signals, respectively, and $x_\Delta(t)=x_2(t)-x_1(t)$, $x_\Sigma(t)=x_2(t)+x_1(t)$. We will then finally have

$$w(t)=c[x_\Delta(t)-Gx_\Sigma(t)],$$

where c and G are coefficients equal to, respectively

$$c=-\frac{N_0+2Nr^2}{N_0+2N(r^2+k^2\alpha_1^2)},\quad G=\frac{2Nrk\alpha_1}{N_0+2Nr^2}.$$

Comparison to threshold L_0 of function L is equivalent to comparison to threshold $L_0/c\eta$ of functional

$$l=\frac{L}{c\eta}=\int_T[y_\Delta(t)-Gy_\Sigma(t)]^2\,dt,$$

where

$$y_{\Delta(\Sigma)}(t)=\int_T\frac{\sin[\pi\Pi(t-s)]}{\pi(t-s)}x_{\Delta(\Sigma)}(s)\,ds.$$

Taking this into account, we arrive at one of the variants for optimum processing of output signals of monopulse radar antennas in the mode of distinguishing the composition of the located target, which is shown schematically in Figure 2. The most significant operations from the viewpoint of joint processing of the received fluctuations are receipt of the difference $x_\Sigma(t)$ and total $x_\Delta(t)$ and formation of the linear combination $y(t) = y_\Delta(t) - Gy_\Sigma(t)$. Taking (1) and (2) into account, it is easy to check

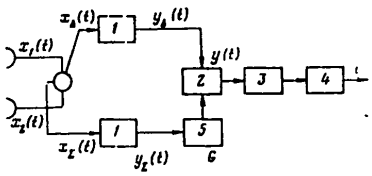

Figure 2. (1--Linear filter; 2--Readout device; 3--Square law function generator; 4--Integrator; 5--Multiplier)

that the linear combination coefficient G for any of the considered hypotheses is equal to the ratio $\overline{y_\Delta(t)y_\Sigma(t)}/\overline{y_\Sigma^2(t)}$, at which the minimum value of $y^2(t)$ is provided. The value of the latter is equal to

$$\overline{y^2(t)} = \overline{y(t)y_\Delta(t)} = \overline{y_\Delta^2(t)} - \frac{\overline{[y_\Delta(t)y_\Sigma(t)]^2}}{\overline{y_\Sigma^2(t)}},$$

and $\overline{y(t)y_\Sigma(t)} = 0$.

The standard deviation $\overline{y^2(t)}$ will be close to that of natural thermal noise (regardless of the specific value of angular coordinate α_1) if there is a single target in the resolved volume of a monopulse radar. Otherwise the value of $\overline{y^2(t)}$ will additionally take into account the angular length of a group target and also the total output of the received signals. Comparison of the output signal of the diagram of Figure 2 to the threshold permits one to establish the fact of the presence of a group target.

We note in conclusion that the discrimination diagram of Figure 2 can also be obtained for other statistical models of received signals.

BIBLIOGRAPHY

1. "Zashchita ot radiopomekh" [Protection Against Radio Noise], edited by M. V. Maksimov, Izd. Sovetskoye radio, 1976.

2. Leonov, A. I. and K. P. Fomichev, "Monoimpul'snaya radiolokatsiya" [Monopulse Radar], Izd. Sovetskoye radio, 1970.

3. Kuz', N. Ya., RADIOTEKHNIKA I ELEKTRONIKA, Vol 17 No 9, 1972.

4. Cook, U. S. Patent No 3130402, dated 12 Feb 1957.

[8144/0508-6521]

6521
CSO: 8144/0508

END